https://doi.org/10.5194/esurf-2021-72
Preprint. Discussion started: 19 October 2021

Earth Surface Dynamics Discussions
Open Access
EGU

Signal response of the Swiss plate geophone monitoring system impacted by bedload particles with different transport modes

Zheng Chen[1,2,3], Siming He[1], Tobias Nicollier[2], Lorenz Ammann[2], Alexandre Badoux[2], Dieter Rickenmann[2]

[1]Institute of Mountain Hazards and Environment, Chinese Academy of Sciences, Chengdu, 610041, China
[2]Swiss Federal Institute for Forest, Snow and Landscape Research WSL, Birmensdorf, 8903, Switzerland
[3]University of Chinese Academy of Sciences, Beijing, 100049, China

Correspondence to: Zheng Chen (zheng.chen@wsl.ch)

Abstract. Controlled experiments were performed to investigate the acoustic signal response of the Swiss plate geophone (SPG) system impacted by bedload particles varying in size, impact angle and transport mode. The impacts of bedload particles moving by saltation, rolling, and sliding were determined by analyzing the experimental videos and corresponding vibration signals. For a particle impact on the bed or on the geophone plates, the signature of the generated signal in terms of maximum amplitude, number of impulses and centroid frequency was extracted from the raw monitoring data. So-called signal packets were determined by performing a Hilbert transform of the raw signal. The number of packets was calculated for each transport mode and for each particle size class, with sizes ranging from 28.1 mm to 171.5 mm. The results show how the number of signal impulses per particle mass, the amplitude of the signal envelope, and the centroid frequency change with increasing particle size, and they also demonstrate the effect of bedload transport mode on the signal response of the SPG system. We found that there is a general increase in the strength of the signal response or in the centroid frequency when the transport mode changes from sliding to rolling to saltation. The findings of this study help to better understand the signal response of the SPG system for different bedload transport modes, and may also contribute to an improvement of the procedure to determine bedload particle size from the SPG signal.

1 Introduction

Quantification of bedload transport processes constitutes a significant challenge in river dynamics and can provide a prerequisite for the design of hydraulic engineering structures and for the assessment of natural hazards (Rickenmann, 2016). Additionally, measurements of bedload transport rates in both laboratory and field help to improve understanding of its transport mechanism and to validate existing models or formulas (Habersack and Laronne, 2002; Schneider et al., 2015; Rickenmann, 2020).

In general, there are two types of methods for measuring bedload transport rate, including (1) direct methods to measure the transported bedload mass, installing physical samplers and traps on the river bed for some time frame (Bunte et al., 2004; Childers, 1999; Emmett, 1980; Hayward, 1980; Helly and Smith, 1971; Gray et al., 2010; Ryan et al., 2005); (2) indirect

https://doi.org/10.5194/esurf-2021-72
Preprint. Discussion started: 19 October 2021

methods, in particular, the acoustic-based monitoring devices, including piezoelectric sensors (Krein et al., 2008; Rickenmann and McArdell, 2007), hydrophones (Barton et al., 2010; Camenen et al., 2012; Rigby et al., 2015, 2016; Geay et al., 2017), pipe microphones (Mizuyama et al., 2010), geophones (Rickenmann et al., 2012, 2014; Rickenmann, 2017) and seismic sensors (Farin et al., 2019; Gimbert, 2019; Roth et al., 2017; Tsai et al., 2012).

The advantage of the indirect bedload measuring method is to provide long-term continuous data on bedload transport (Rickenmann, 2017). In comparison, the direct bedload measuring method is suited for gravel-bed streams under the condition of low- or medium-discharge levels and typically relatively short sampling duration (Gray et al., 2010), and taking bedload samples can be challenging in case of large flow discharges and steep streams (Rickenmann and Fritschi, 2017; Nicollier et al., 2019). However, the indirect measurements must be calibrated using the direct methods (Wyss et al. 2016a, 2016b).

Acoustic-based indirect devices record the vibration signals generated by bedload particles impacting on a stream bed, an impact plate, or an impact pipe (Rickenmann, 2017). The acoustic vibration signal contains information, e.g. in terms of amplitude, impulses and characteristic frequency (Barton et al., 2006; Burtin et al., 2008, 2010, 2011; Govi et al., 1993; Hsu et al., 2011; Tsai et al., 2012; Vasile, 2020), which can be used to infer the bedload transport rates (Wyss et al., 2016a, 2016b; Nicollier et al., 2020). One such method, the Swiss plate geophone (SPG) system is a robust monitoring device that records the acoustic signal generated by bedload particle impacting onto steel plates. The SPG system was deployed at more than 20 field sites, mainly across Europe (Rickenmann, 2017), aiming to derive bedload fluxes and particle size distributions (Wyss et al., 2016c). Significant differences between field-based calibration relationships were found to be possibly caused by variations of particle impact location and impact angle (Turowski et al., 2013), particle shape (Cassel et al., 2021; Krein et al., 2008), streamflow velocity (Rickenmann et al., 2014; Wyss et al., 2016a), grain size distribution (Nicollier et al., 2021a), and particle transport mode (Krein et al., 2008; Turowski and Rickenmann, 2009; Turowski et al., 2015).

In addition to field calibration measurements, controlled flume experiments were conducted with different types of acoustic devices (Beylich and Laute, 2014; Moen et al., 2010; Mizuyama et al., 2010; Wyss et al., 2016a), to investigate their suitability for monitoring of bedload transport with variable transport modes (Tsakiris et al., 2014). In particular, the bedload transport modes, namely, saltation, rolling and sliding, influence the acoustic signal response of geophones or other acoustic sensors (Tsakiris et al., 2014), thus affecting the signal-bedload calibration relations. Previous studies have shown that the transported particles in the mode of rolling and sliding are associated with a more important signal power at lower frequencies compared to salting particles (Krein et al., 2008; Thorne, 1985). This finding was also supported by a flume experiment with a geophone impact plate, using unisize spherical glass beads with different transport modes (Tsakiris et al., 2014). Additionally, the signal responses of the geophone were observed to depend both on flow conditions and on transport modes (Tsakiris et al., 2014). It is therefore important to quantify the effect of the transport mode on the signal response, as this will eventually affect the signal-based particle size classification.

Controlled outdoor flume experiments with the SPG system (Nicollier et al., 2021) were carried out to better understand the influence of transport mode. However, flow conditions (turbidity, illumination) sometimes impaired the clarity of the

https://doi.org/10.5194/esurf-2021-72
Preprint. Discussion started: 19 October 2021

videos that were recorded by a camera during the experiments to capture the motion characteristics of bedload particles. A way to extend the experimental data is to apply the finite element method (FEM), which has been used already successfully to simulate the structural dynamic responses of the SPG system impacted by a quartz sphere falling vertically onto the SPG plate (Chen et al., 2021). The FEM simulation is used here also for non-vertical impacts to investigate the effect of different bedload impact angles, covering a wide range of angles for transport modes (saltation, rolling, and sliding) observed in the flume experiments.

The aim of the present paper is to investigate how the signal response of the SPG system impacted by bedload particles changes for different transport modes. First, controlled flume experiments and inclined chute experiments were performed with natural bedload particles and quartz spheres. On the basis of the video material recorded during these experiments, we compared for each impact event the motion of the bedload particles, including transport mode, impact position, and impact instant with the acoustic signal recorded by the SPG system. Second, a FEM model of the SPG system was used to simulate the signal response of the SPG system produced by quartz spheres with varying impact angles ranging from 0° to 90° for different particle sizes, and the results were compared with the observations from the inclined chute experiment. Data from the physical experiments and the numerical simulations were analyzed quantitatively in terms of signal responses for each transport mode and for changing particle size.

2 Methods

2.1 Controlled experiments

2.1.1 Experimental set-up

Full-scale controlled flume experiments were performed with natural bedload particles varying in size (Nicollier et al., 2019, 2020, 2021a), using an outdoor experimental facility at the Oskar von Miller Institute of the Technical University of Munich in Obernach, Germany. The entire experimental system can be divided into serval parts including the flume channel made of concrete, the measuring reach equipped with different types of sensors (**Fig. 1a**), namely the Swiss plate geophone (SPG) system, the miniplates accelerometer (MPA) and the Japanese pipe microphone (JPM), and the basin for collecting and recycling bedload particles. This experimental system enables quantitative investigations regarding the process of bedload transport, observing the characteristics of the particles motion and measuring the vibration signals during the bedload transport process. The experimental channel reach used in this study has a rectangular cross-section, a length of 24 m, a width of 1.02 m, a maximum depth of 2.02 m and a slope of 4% (Nicollier et al., 2019). The channel bed roughness is made up by gravel particles that have a size corresponding to D_{67} and D_{84} of the bedload material sampled in the field, embedded in concrete and about half their size protruding into the flow. The SPG system is installed in the measuring reach (**Fig. 1a**) with the plates mounted flush with the channel bed and with the geophone sensor recording the vertical vibration (displacement velocity) of the plate. The side wall of the measuring reach is made up by plexiglass for video observation.

https://doi.org/10.5194/esurf-2021-72
Preprint. Discussion started: 19 October 2021

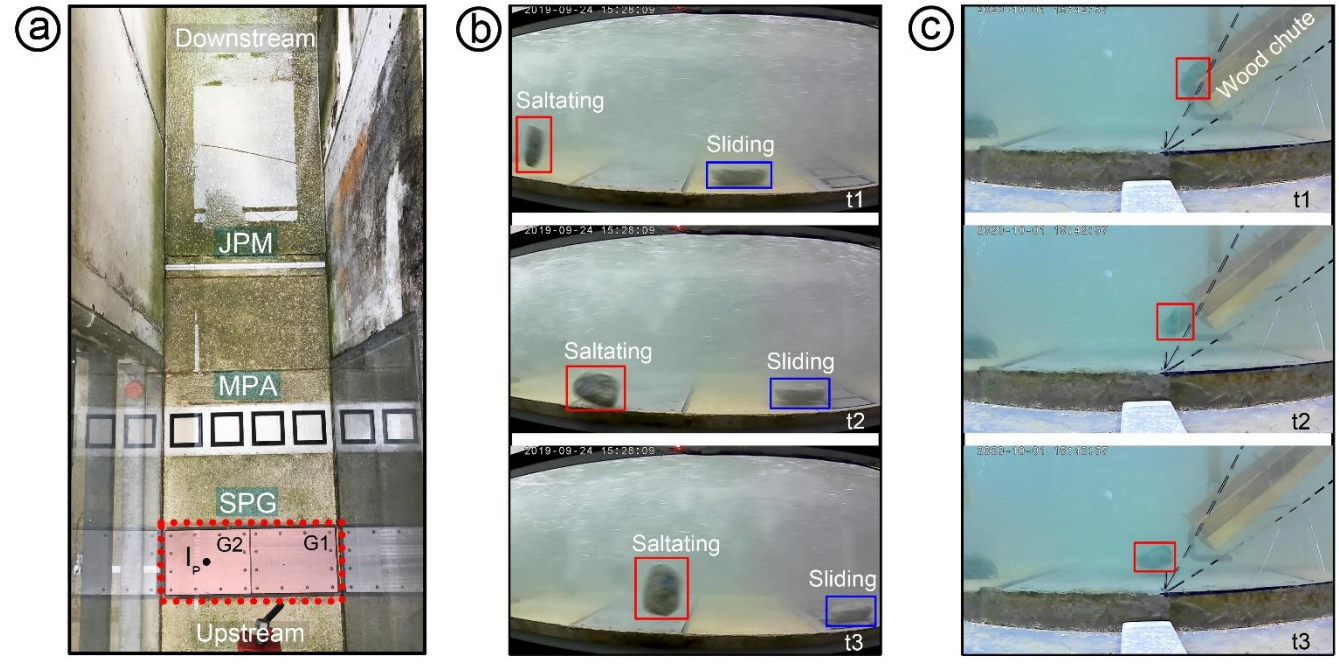

Figure 1: Measuring site at the Obernach experimental flume. (a) Measuring reach with different types of sensors mounted on the flume bed, including the Swiss plate geophone (SPG), the miniplate accelerometer (MPA) and the Japanese pipe microphone (JPM). (b) Frames from video recorded during a controlled flume experiment, used for the tracking of particles (mean b-axis = 127.9 mm) impacting onto and moving over the SPG plates. The particle marked with the red rectangle is transported in saltation, while the one marked with the blue rectangle is sliding. (c) Frames from video recorded during a drop experiment with a wood chute inclined at an angle of 45°. G1 and G2 in (a) are two plates of the SPG system, and the black dot I_P marks the impact location of the bedload particles on the plate G2 for the inclined chute experiments. The time interval between consecutive frames for each column in (b) and (c) is 1/3 s. The length of the geophone plate in flow direction is 0.36 m.

2.1.2 Flume experiments

During the flume experiments, the experimental flow rate was maintained constant, with a flow depth of about 0.54 m and the flow velocity set to 3.3 m/s and monitored using a flow meter (OTT MFpro) positioned 0.1 m above the SPG plate in the middle of the cross-section. The bedload particles with a natural shape were released into the flume several meters upstream of the SPG system. A Lenco camera was set in a side view perpendicular to the plexiglass side wall to record videos with 30 frames per second (FPS) throughout the duration of each experiment. **Fig. 1b** shows typical images of two different particles of size class C9, moving over the SPG plates. The video recordings were analyzed frame by frame and the instants of bedload particle impacts on the concrete bed and the SPG plates were determined. In addition, the transport modes of the particle were assessed from the videos (i.e. saltation, rolling or sliding, as illustrated in **Fig. 3**). The experimental particles were sorted into 10 size (C1 to C10) classes ranging from 12.3 mm to 171.5 mm (**Tab. 1**). In this study, only the data obtained from experiments involving the particle size class C4 to C10 are presented. Particle impacts for the size classes C1

https://doi.org/10.5194/esurf-2021-72
Preprint. Discussion started: 19 October 2021


Earth Surface Dynamics Discussions Open Access EGU

to C3, ranging from 12.3 mm to 21.8 mm, were difficult to distinguish due to (1) poor lighting conditions resulted in low contrast in the video frame image, and (2) the large number of small-sized particles for each experimental run.

Table 1: Bedload particle characteristics for each grain size class *j*.

Bedload size class *j* [-]	Mean size D_j [mm]	Mean particle mass M_j [kg]	Number of particles for each run *n* [-]
C1	12.3	0.003	50
C2	17.4	0.010	50
C3	21.8	0.019	40
C4	28.1	0.041	33
C5	37.6	0.094	20
C6	53.2	0.265	20
C7	71.3	0.574	20
C8	95.5	1.249	10
C9	127.9	3.633	5
C10	171.5	8.743	5

2.1.3 Inclined chute experiments

Significant differences between transport modes (saltation, rolling, and sliding) were observed with regard to the impact angle on the channel bed. Therefore, an inclined chute experiment was conducted in still water to examine the effect of particle impact angle on the signal response of the SPG system (**Fig. 1c**). The length of the chute was 1.0 m and the width was about 0.1 m. Due to the solid friction it was difficult for the particles released at the top of the wood chute to keep moving at small chute angles. Hence, the experimental angles in this study were chosen as 45° and 60° for natural bedload particles with sizes ranging from 12.3 mm to 95.5 mm (where the size is given as the b-axis of the particle) and for spherical particles with sizes ranging from 20 mm to 82 mm. For each test, the flow velocity was around 0 m/s (no flow) and the water depth was 0.84 m. The impact velocity of the bedload particle on the SPG plates was determined to be about 3.7 m/s and 4.1 m/s for chute angles of 45° and 60°, respectively, considering the energy conservation law or estimated using the experimental video frames.

Table 2: Mean particle size D_j and mass M_j and number of test repetitions *m* for bedload particle size class *j* for the impact experiments with channel angles of 45° and 60°. S1, S2, S3, and S4 refer to four quartz spheres of increasing size.

Bedload size class *j* [-]	Mean size D_j [mm]	Mean mass M_j [kg]	Number of tests *m* [-]	Chute slope angle θ [°]
C1	12.3	0.003	10	45°, 60°
C2	17.4	0.010	10	45°, 60°
C3	21.8	0.019	10	45°, 60°
C4	28.1	0.041	10	45°, 60°
C5	37.6	0.094	10	45°, 60°
C6	53.2	0.265	10	45°, 60°

https://doi.org/10.5194/esurf-2021-72
Preprint. Discussion started: 19 October 2021

Earth Surface Dynamics Discussions
Open Access
EGU

C7	71.3	0.574	10	45°, 60°
C8	95.5	1.249	10	45°, 60°
S1	20.0	0.012	5	45°, 60°
S2	31.0	0.050	5	45°, 60°
S3	51.0	0.185	5	45°, 60°
S4	82.0	0.760	5	45°, 60°

2.2 Numerical simulations

To supplement the experimental data, particularly for smaller impact angles, a finite element method (FEM) was built to produce a virtual model of the SPG system, as illustrated in **Fig. 2.** The FEM model includes structural components of the SPG system, such as the steel plate, bolts, sensor casings, elastomers, and the internal and outer frames were subdivided, individually, into small finite elements. Subsequently, all the components were assembled considering mechanical contacts and frictions, and the entire SPG system was simulated in the LS-DYNA (LSTC 2014). Detailed information used in the FEM model are reported by Chen et al. (2021). The FEM model was used to numerically simulate the signal response for spherical particles impacting a SPG plate with a speed of 3.5 m/s (irrespective of the impact angle) at different angles ranging from 0° to 90°, and for sphere diameters of 82 mm, 95.5 mm, and 120 mm, as indicated in **Tab. 3**.

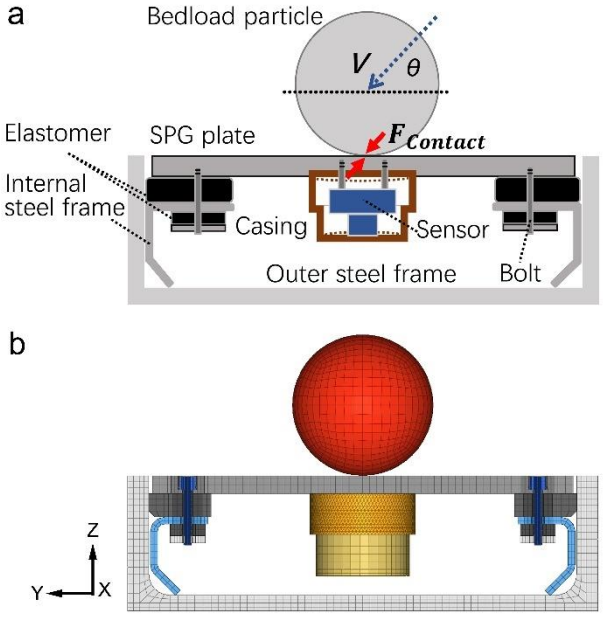

Figure 2: (a) Cross-sectional sketch of the SPG system impacted by a spherical particle. (b) Cross-sectional of the FEM model of the SPG system. The coordinate system is set up with the X-axis pointing in the transverse direction (across the flume width), the Y-axis pointing downstream (in flow direction), and the Z-axis pointing up perpendicularly to the plate's surface. θ is the impact angle of the sphere. $F_{Contact}$ is the contact force between the sphere and the plate. V is the impact velocity of the sphere onto the plate, which has two components V_Y and V_Z given in Tab. 3.

https://doi.org/10.5194/esurf-2021-72
Preprint. Discussion started: 19 October 2021

Earth Surface Dynamics Discussions
Open Access
EGU

Table 3: Characteristic values of the spheres and impact angles used in the FEM simulations. The diameters D_1, D_2 and D_3 of the spheres are 82 mm, 95.5 mm and 120 mm, respectively. A constant density ρ_s = 2677 kg/m^3 was used in the FEM simulations. V_Y and V_Z are the components of the impact velocity in the Y and Z directions, respectively.

No.	D_1 [mm]	D_2 [mm]	D_3 [mm]	Impact angle [°]	V_Y [m/s]	V_Z [m/s]
1	82.0	95.5	120.0	0	3.500	0.000
2	82.0	95.5	120.0	10	3.447	0.608
3	82.0	95.5	120.0	20	3.289	1.197
4	82.0	95.5	120.0	30	3.031	1.750
5	82.0	95.5	120.0	45	2.475	2.475
6	82.0	95.5	\	60	1.750	3.031
7	82.0	95.5	\	70	1.197	3.289
8	82.0	\	\	80	0.608	3.447
9	82.0	\	\	90	0.000	3.500

2.3 Bedload transport modes

2.3.1 Saltation, rolling and sliding

Generally, the bedload particles are transported in three types of motions, namely saltation, rolling and sliding, as illustrated in **Fig. 3**. In other studies, the motion mode of the bedload transport was investigated experimentally and showed a correlation with the time-averaged bed shear stress $\overline{\tau_b}$ or the ratio of $\overline{\tau_b}$ to the critical value of the bed shear stress $\tau_{critical}$ for incipient particle motion (Tsakiris et al., 2014). The value of $\overline{\tau_b}$ is constant in the case of the uniform flow condition, which can be calculated as

$$\overline{\tau_b} = \rho g R_h S \,, \tag{1}$$

where ρ is the water density, g is the gravity acceleration, S is the bed slope, and R_h is the hydraulic radius that can be expressed as $bh/(2h+b)$ for a rectangular cross section, h is the flow depth, and b is the channel width. For our flume experiments, $\overline{\tau_b}$ is determined as 102.9 N/m^2.

The critical Shields parameter $\Theta_{Critical}$ is defined as the ratio of the critical bed shear stress $\tau_{critical}$ to the submerged particle weight:

$$\Theta_{Critical} = \frac{\tau_{Critical}}{(\rho_s-\rho)gD} \,, \tag{2}$$

where ρ_s is the particle density.

Then the excess transport stage T (Auel et al., 2017) can be calculated by **Eq. 3**:

$$T = \frac{\overline{\tau_b}}{\tau_{Critical}} - 1 = \frac{R_h S}{\Theta_{Critical}\left(\frac{\rho_s}{\rho}-1\right)D} - 1 \,, \tag{3}$$

Studies have showed that the probability of transport mode P_M (P_{Sal}, P_{Rol}, and P_{Sli} for saltation, rolling, and sliding, respectively) is related to the flow intensity or T (Auel et al., 2017; Hu and Hui, 1996a). The critical Shields parameter

https://doi.org/10.5194/esurf-2021-72
Preprint. Discussion started: 19 October 2021

Earth Surface Dynamics Discussions
Open Access
EGU

$\Theta_{Critical}$ in our flume experiments is assumed as 0.03, as determined by Schneider et al. (2015) for mountain streams, and by Shahmohammadi et al. (2021) for flume experiments. For our flume experiments, T is calculated ranging from 0.22 to 6.42 for the particle size ranging from 171.5 mm to 28.1 mm.

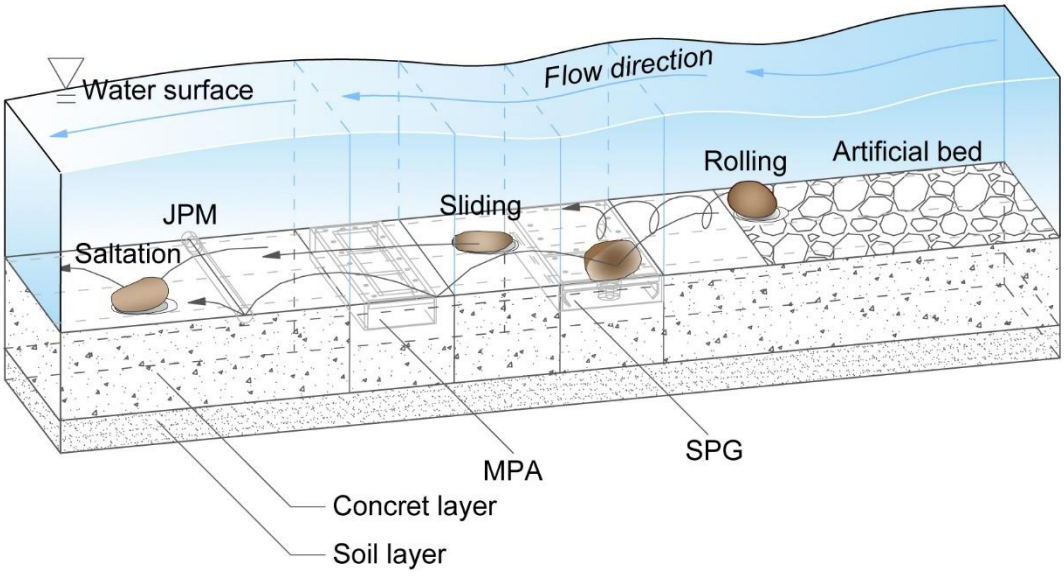

Figure 3: Sketch of bedload particles in different transport modes, including saltation, rolling and sliding, moving over the Obernach flume facility.

2.3.2 Impact instant and video analysis

In order to match the transport mode of a bedload particle with the vibration signal, an important parameter that needs to be determined from experimental videos is the time instant when a particle impacts onto the channel bed. **Figs. 4a-4c** show sketches of transport modes of saltation, rolling and sliding, respectively, and also indicate an interaction between the bedload particle and the SPG plate. A shear stress between the geophone plate and the contact surface of a particle is generated when the particle impacts onto the plate with a certain angle, as seen in **Fig. 4a**. The frictional force $\boldsymbol{F_c}$ together with the fluid drag force $\boldsymbol{F_w}$ form a force couple. Similarly, another set of force couple is present in the vertical direction, namely the vertical support force $\boldsymbol{F_n}$ and the particle weight force $\boldsymbol{G}$. These force couples act together on the particle, and finally rotate the particle. This small rotation of the bedload particle occurs immediately after impacting, allowing to determine the impact instant (at T_1) from the video frames. **Appendix A** gives more details on how we analyzed the experimental videos.

https://doi.org/10.5194/esurf-2021-72
Preprint. Discussion started: 19 October 2021

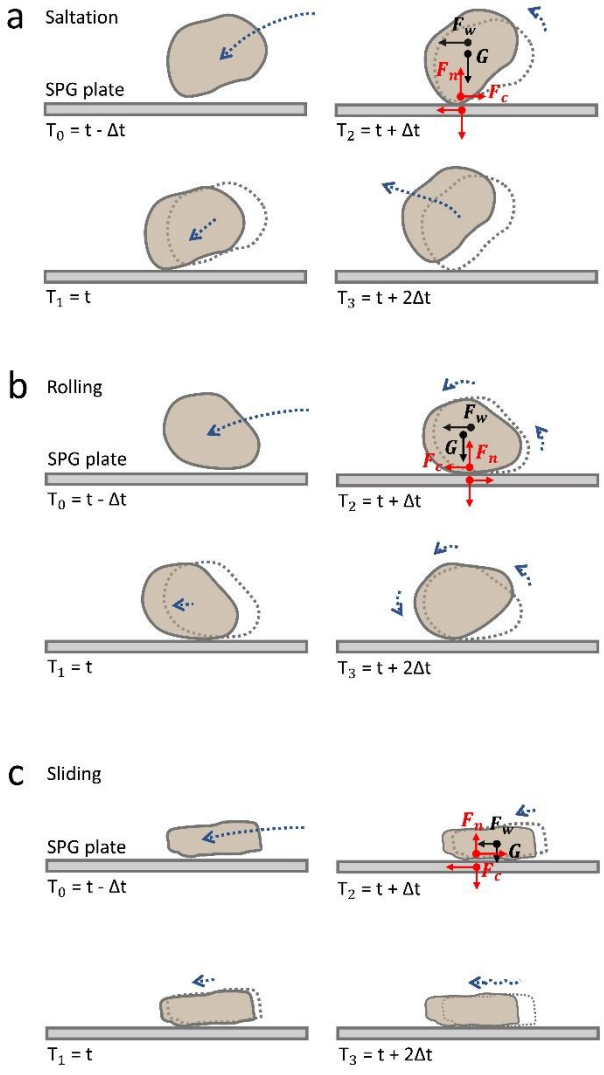

Figure 4: Schematic illustration of the three observed types of transport modes: (a) saltation, (b) rolling and (c) sliding. T_0, T_1, T_2, and T_3 are four different time instants of particle motion, indicating impact and rebound of a particle on the SPG plate. In particular, T_2 is the instant when the bedload particle impacts on the SPG plate. $\boldsymbol{F_c}$ and $\boldsymbol{F_n}$ denote a friction force and a vertical support force exerted by the SPG plate on the bedload particle, respectively. $\boldsymbol{F_w}$ is a force of water acting on the bedload particle. $\boldsymbol{G}$ is particle weight force.

2.4 Signal processing

2.4.1 Signal characteristics: amplitude, impulse, frequency

A typical signal response of the SPG system recorded during a flume experiment for the bedload particles of grain-size class C9 moving over the SPG plates is illustrated in **Fig. 5**. The packets (**Figs. 5a** and **5b**) were delimited on the basis of the envelope (blue line) of the signal computed with Hilbert transform (Wyss et al., 2016a). Each packet corresponds to the

https://doi.org/10.5194/esurf-2021-72
Preprint. Discussion started: 19 October 2021

signal response following a single particle impact onto the SPG plate, as seen in **Fig. 5c**. Subsequently, these packets were classified according to the respective transport modes of saltation (in gray), rolling (in red) and sliding (in blue), as determined from the experimental videos that were introduced above. The packets colored in purple suggest that the signals of this packet recorded by the sensor G1 or G2 were triggered by impacts on the neighboring sensor G2 or G1, respectively, or they represent the signals that cannot be matched with the videos due to limitation of light conditions.

The positive maximum amplitude of a packet is given as $Amp_{Max,\ Pac}$ (V), as seen in **Fig. 5c**. The number of impulses I (**Fig. 5d**) of each packet is obtained by counting the times of positive signal excursions above the pre-defined system threshold (Rickenmann et al., 2012, 2014; Wyss et al., 2016a). The threshold value in our study is 0.0216 V, as indicated by the blue dash-dotted line in **Fig. 5d**.

The mass-impulse coefficient k_{IPM} was used as a parameter relating the signal strength to the transported bedload mass M (Chen et al., 2021), and is defined as the number of impulses per particle mass:

$$k_{IPM} = \frac{I}{M}, \tag{4}$$

where I is the number of signal impulses recorded by the SPG system and M is the corresponding transported particle mass. According to the Hertz theory, the centroid frequency $Freq_{centroid}$ (**Eq. 5**) of the SPG signal is an important parameter that can help to support the bedload size identification (Wyss et al., 2016a; Rickenmann, 2017; Thorne, 2014):

$$Freq_{Centroid} = \frac{\sum f_m A_{FFT,m}}{\sum A_{FFT,m}}, \tag{5}$$

where f_m is the spectrum frequency (Hz) and $A_{FFT,m}$ is the amplitude (V·s) that is obtained by performing fast Fourier transform FFT on the signals.

https://doi.org/10.5194/esurf-2021-72
Preprint. Discussion started: 19 October 2021

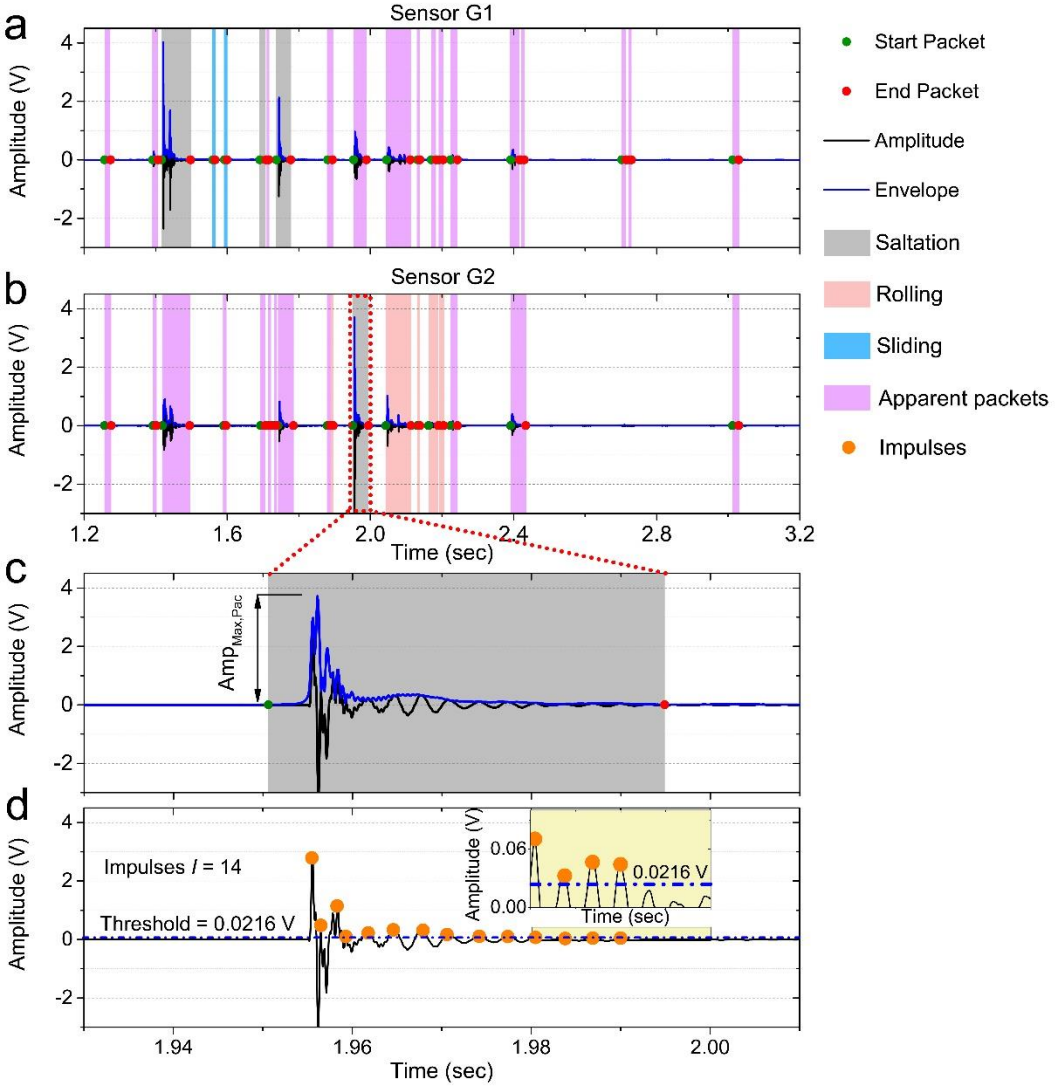

Figure 5: Illustration of the SPG vibrations and signal packets for different transport modes following a flume experiment with bedload particles of grain-size class C9. (a) and (b) represent signals that were recorded by geophone sensor G1 and G2, respectively, with a flow velocity of 3.3 m/s. (c) Illustration of the packet definition as the envelope (blue line) of the raw signal, computed with the Hilbert transform, and representing one impact of a saltating particle. (d) Definition of impulse counts I (= 14), counting the times the signal exceeds the threshold (0.0216 V, see the blue dash-dotted line) in the positive domain.

2.4.2 Number of packets

The amplitude and frequency characteristics of the signal were found to vary significantly with the impact locations of the bedload particle, in particular when an impact occurs on a neighboring plate or on the concrete bed of the channel. An amplitude-frequency-based filtering method has been developed by Nicollier et al. (2021b, in review) to identify packets generated by these impacts and to classify them as “apparent”. In contrast, packets generated by bedload particles impacting

https://doi.org/10.5194/esurf-2021-72
Preprint. Discussion started: 19 October 2021

on the SPG plate above the considered geophone sensor are being classified as "real". This filtering process accounts for the phenomenon of attenuation acting on a propagating seismic wave. In fact, the further a seismic wave propagates, the stronger is the attenuation of high frequencies with regard to low frequencies and thus the lower is the energy of the wave. "Apparent" packets can therefore be identified and removed from the final packet counting on the basis of their low amplitude-frequency content.

Subsequently, the ratio $r_{i,j}^{Packet,V\_F}$ of the total number of real packets over all transport modes based on the video observations to the real-packet number determined by the filtering method is calculated by

$$r_{i,j}^{Packet,V\_F} = \frac{N_{i,j}^{Packet,V}}{N_{i,j}^{Packet,F}}, \quad (6)$$

where $N_{i,j}^{Packet,V}$ is the total number of real packets for experimental run i and grain-size class j over transport modes based on the video analysis; $N_{i,j}^{Packet,F}$ is the number of real packets for experimental run i and grain-size class j, determined by the filtering method.

In addition, similar to the definition in Wyss et al. (2016c), the ratio $\alpha_{i,j}^{Packet}$ of the number of packets $P_{i,j}$ to the number of particles $N_{i,j}$ for each experimental run i and grain-size class j is given as:

$$\alpha_{i,j}^{Packet} = \frac{P_{i,j}}{N_{i,j}}, \quad (7)$$

For each transport mode, using all detected packets including both "real" and "apparent" packets, we have:

$$\alpha_{i,j}^{Packet,Mode} = \frac{P_{i,j}^{Mode}}{N_{i,j}^{Mode}}, \quad (8)$$

where $\alpha_{i,j}^{Packet,Mode}$ are the ratios of the number of packets to the number of particles for experimental run i and particle-size class j for the transport mode of saltation, rolling and sliding; $P_{i,j}^{Mode}$ and $N_{i,j\,j}^{Mode}$ are the numbers of packets and transported particles for experimental run i and particle-size class j for the mode of saltation, rolling and sliding, respectively.

2.4.3 Estimation of particle velocity

Generally, the value of bedload particle velocity V_P is expected to be less than the water flow velocity V_W. If the ratio $r_{PW} = V_P/V_W$ and V_W are given, then V_P can be estimated by the following equation:

$$V_P^{Est} = r_{PW} V_W, \quad (9)$$

where V_P^{Cal} is called the estimated particle velocity in present study; r_{PW} ranges from 0.3 to 0.8 for natural particles as suggested by Julien and Bounvilay (2013).

V_P can be also calculated by particle travel distance L_P and time ΔT_P, which is expressed as:

$$V_P^{Cal} = \frac{L_P^{SPG,MPA}}{\Delta T_P^{SPG,MPA}}, \quad (10)$$

https://doi.org/10.5194/esurf-2021-72
Preprint. Discussion started: 19 October 2021

Earth Surface Dynamics Discussions
Open Access
EGU

where V_P^{Cal} is called calculated particle velocity in this study; $L_P^{SPG,MPA}$ is a constant of 0.775 m, determined by the centre-to-centre distance between the SPG and MPA systems; $\Delta T_P^{SPG,MPA} = T_P^{MPA} - T_P^{SPG}$ is the arrival time difference determined from the starting time of the packets T_P^{SPG} and T_P^{MPA} for the SPG and MPA systems, respectively. More details about the calculation of $\Delta T_P^{SPG,MPA}$ can be found in **Appendix B**.

To compare our experiments data with the other flume studies, the particle velocities introduced above are normalized as:

$$V_P^{M,*} = \frac{V_P^M}{\sqrt{(s-1)gD}}, \tag{11}$$

where $V_P^{M,*}$ represents the nondimensional particle velocity, i.e. $V_P^{Est,*}$ or $V_P^{Cal,*}$, indicating the particle velocity normalized by the term $\sqrt{(s-1)gD}$; s is the ratio of particle density ρ_s to water density ρ.

3 Results

3.1 Percentage distribution of transport modes

To assess signal signatures of the SPG system impacted by bedload particles varying in transport mode, a total of 2414 bedload impacts were analyzed for particles ranging in size (b-axis) from 28.1 mm to 171.5 mm (size classes C4 to C10) under a constant flow condition. **Fig. 6a** shows the total number of impacts for each bedload grain size class, including the real impacts for the modes of saltation, rolling and sliding. The apparent impacts and the impacts that generate no packets are both included in the category "other impacts". Out of the total number of impacts, the percentage of the number of real impacts (= real packets) ranges from 22% to 31% generally increases with increasing particle size. As a consequence, the total number of real impacts over all particle sizes is calculated to be 571. Obviously, the number of effective impacts (= real impacts + apparent impacts) for all transport modes is larger than that of the real impacts, considering all impact locations including the concrete bed and the SPG plates, as seen in **Fig. 6b**.

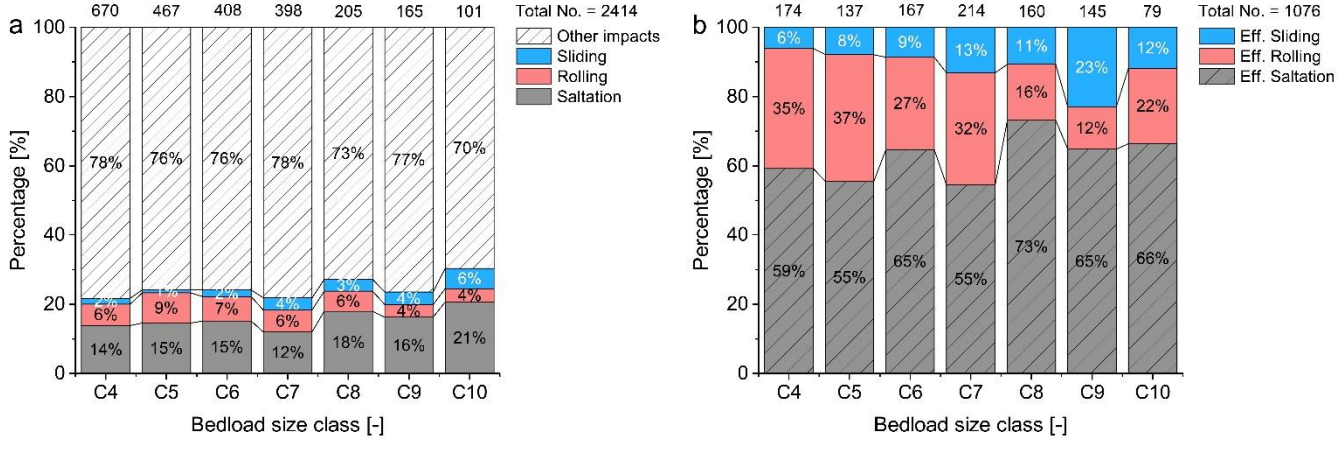

https://doi.org/10.5194/esurf-2021-72
Preprint. Discussion started: 19 October 2021

Earth Surface Dynamics Discussions
Open Access
EGU

Figure 6: Percentage of impacts number for the transport mode of saltation, rolling and sliding. (a) The total impacts and the percentage of real impacts on the geophone plates for each transport mode. (b) The percentage of effective impacts for all transport modes anywhere on the bed or plates. The abbreviation Eff. refers to the effective impacts or packets. The number at the top of each column represents the total impact number for each particle size class.

The value of $r_{i,j}^{Packet,V\_F}$ is slightly smaller than but close to one for small particle sizes ranging from 28.1 mm to 71.3 mm, (**Fig. 7)**, indicating that the number of real packets based on the video analysis is smaller than that obtained from the filtering method using the amplitude-frequency information as introduced above. However, for the largest three particle size classes, the value of $r_{i,j}^{Packet,V\_F}$ generally increases with increasing particle size.

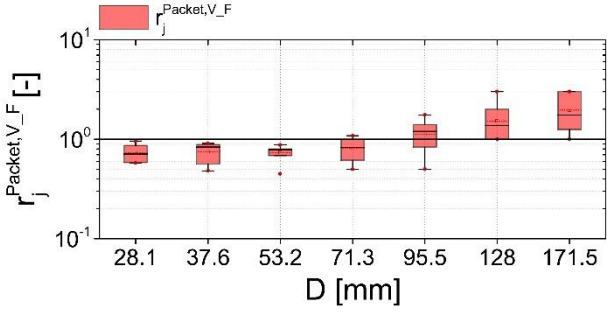

Figure 7: The ratio $r_{i,j}^{Packet,V\_F}$ of total number of real packets for all transport modes based on the video analysis to the number of real packets determined by the filtering method for each particle size class *j*.

3.2 Signal responses of the SPG system

In the following, we present the summary statistics of the coefficient k_{IPM} (number of signal impulses per particle mass), the maximum amplitude $Amp_{Max,Pac}$ and the centroid frequency $Freq_{Cenroid}$ as a function particle size or impact angle, respectively, for different transport modes. A constant impact speed of 3.5 m/s for the spheres was used in the FEM simulations, resulting in different vertical impact velocities for different impact angles onto the plate (**Tab. 3**).

https://doi.org/10.5194/esurf-2021-72
Preprint. Discussion started: 19 October 2021

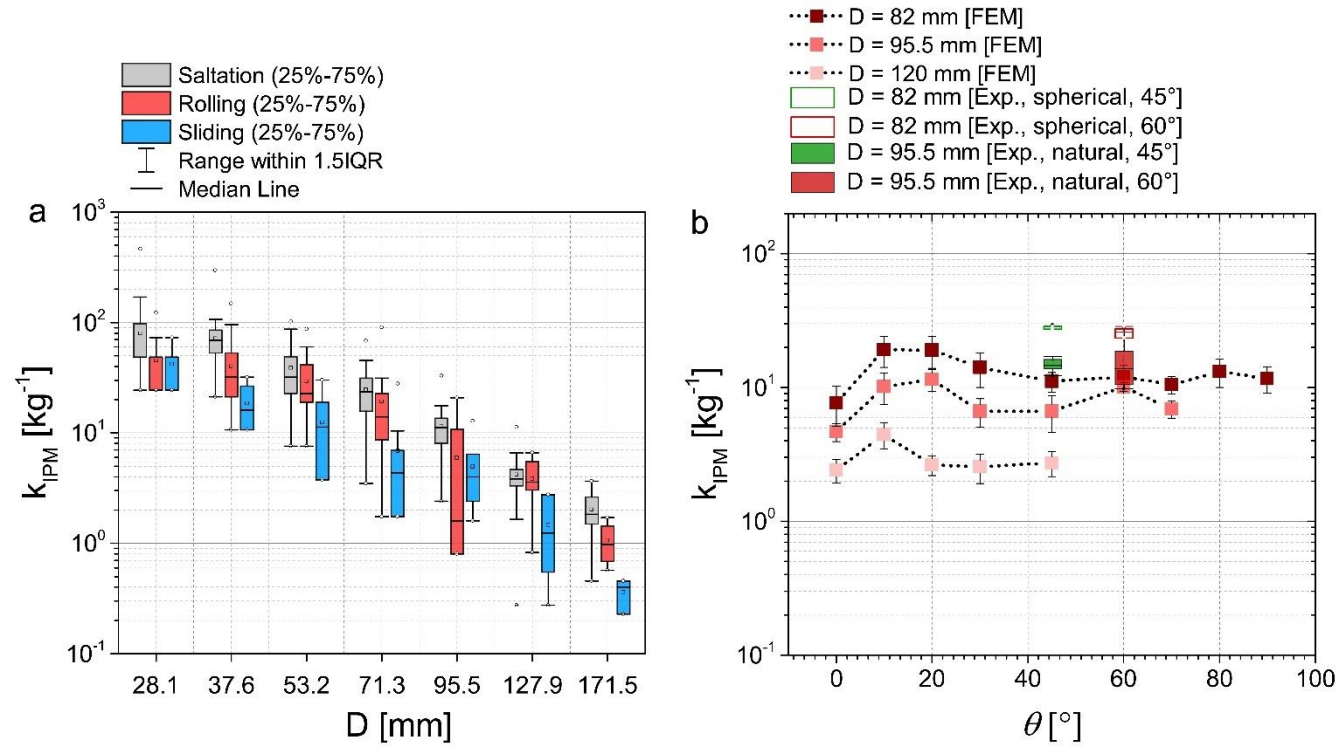

Figure 8: (a) Impulse-mass coefficient k_{IPM} versus bedload particle size D (b-axis) for different transport modes. (b) Impulse-mass coefficient k_{IPM} versus the impact angle θ for different impacting particle sizes. While FEM denotes simulations with the finite element method, the abbreviation Exp. refers to the inclined chute experiments.

The coefficient k_{IPM} decays strongly with increasing particle size D, regardless of whether the particles are in saltation, rolling or sliding motion (**Fig. 8a**). On average the k_{IPM} values of saltation particles are larger than those of rolling particles, and the sliding particles tend to have the lowest values. The overlap of the k_{IPM} values for particles in different transport modes varies between particle sizes which makes it difficult to distinguish motion modes by only considering the value of k_{IPM}.

Both the inclined chute experiments and the FEM simulations indicate that the impulse-mass coefficient k_{IPM} varies only moderately with impact angle for a given particle size, except for impact angles changing from 0° to 10° for the FEM model (**Fig. 8b**). In contrast, the coefficients k_{IPM} decrease with increasing sphere size. This is in an agreement with results from the flume experiments with natural particles (**Fig. 8a**).

https://doi.org/10.5194/esurf-2021-72
Preprint. Discussion started: 19 October 2021

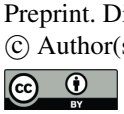

Earth Surface Dynamics Discussions
Open Access
EGU

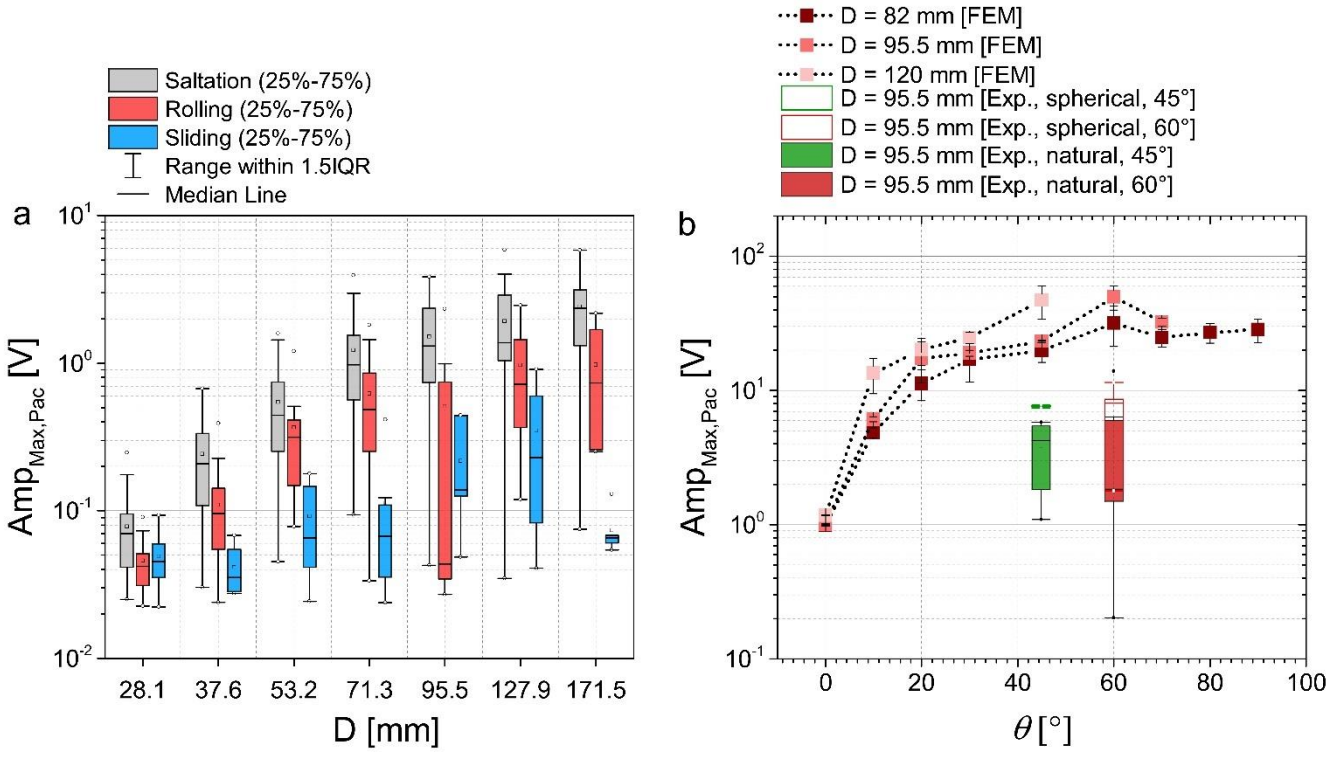

Figure 9: (a) Maximum amplitude $Amp_{Max,\ Pac}$ versus bedload particle size D for different transport modes. (b) $Amp_{Max,Pac}$ versus impact angle θ for different particle sizes. While FEM denotes simulations with the finite element method, the abbreviation Exp. refers to the inclined chute experiments.

The maximum amplitude of a packet $Amp_{Max,Pac}$ generally increases with increasing bedload particle size D for all transport modes (**Fig. 9a)**. The saltation particles tend to generate the largest signal amplitudes, followed by the rolling particles and then the sliding particles. The sliding particles do not display a very clear relation between $Amp_{Max,\ Pac}$ and D.

The maximum amplitude of a packet $Amp_{Max,Pac}$ increases with increasing particle impact angle θ up to about $\theta = 60°$. The FEM simulations and the inclined chute experiments for sphere impacts (**Fig. 9b)** show a similar trend but no clear trend for natural particles.

https://doi.org/10.5194/esurf-2021-72
Preprint. Discussion started: 19 October 2021

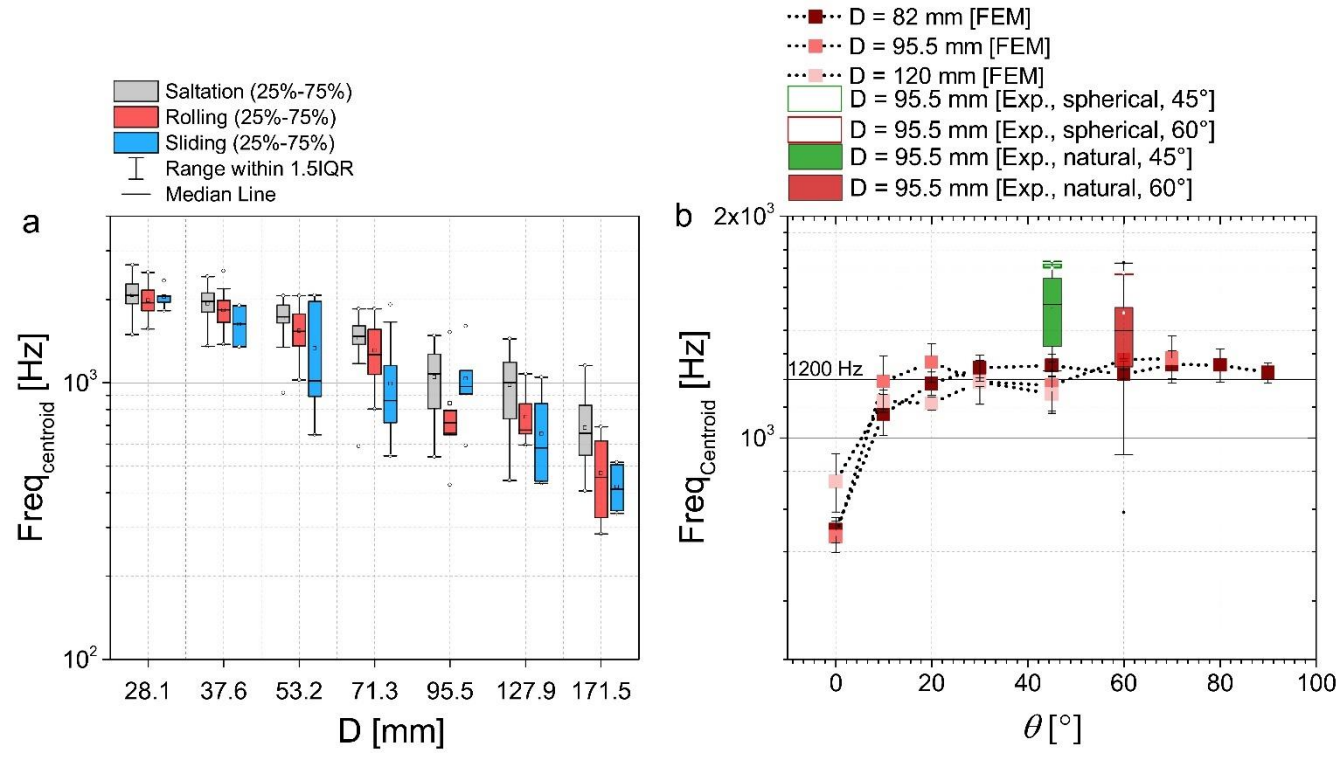

Figure 10: (a) Centroid frequency $Freq_{Centroid}$ versus bedload particle size D for different motion modes. (b) Centroid frequency $Freq_{Centroid}$ versus impact angle θ for different impacting particle sizes. While FEM denotes simulations with the finite element method, the abbreviation Exp. refers to the inclined chute experiments.

320 The centroid frequency $Freq_{Centroid}$ generally decreases with increasing D for all transport modes (**Fig. 10a**). Similar to the maximum amplitude, $Freq_{Centroid}$ values for saltation particles are generally largest, followed by values for the rolling and then the sliding particles. However, it appears that the discriminating effect of particle transport mode on the centroid frequency is rather weak for some particle sizes. The variability in frequency for each transport mode may also be partly due to variable particle impact locations on the geophone plate. Other factors, such as the particle shape can also play a role.

325 According to the FEM simulations, the centroid frequency $Freq_{Centroid}$ increases with impact angle up to about θ = 20° (**Fig. 10b)**. The data from the inclined chute experiments show a slight decrease of $Freq_{Centroid}$ for the largest of the two tested impact angles.

https://doi.org/10.5194/esurf-2021-72
Preprint. Discussion started: 19 October 2021

4 Discussion

4.1 Effect of transport mode on the SPG signal response

4.1.1 Number of packets for each transport mode

We showed that the ratio between the total number of real packets based on the video analysis and the number of packets resulting from the filtering method (Nicollier et al., 2021b, in review) $r_{i,j}^{Packet,V\_F}$ is slightly smaller than but close to one for particle sizes ranging from 28.1 mm to 71.3 mm (**Fig. 7)**. This is due to the fact that in the experiment, only the particle impacts that are on the SPG plates are selected. The signal that is produced by the impacts on the concrete is dampened during wave propagation and filtered using the numerical method. Note that, for the real impacts, the number of packets is equal to the number of impacts, while this is not true especially for the impacts on the concrete due to the non-effective impact. However, the value of $r_{i,j}^{Packet,V\_F}$ increases with increasing particle size ranging from 95.5 mm to 171.5 mm, and approaches a value of around two for the largest particle size class, which is possibly because of the high impact energy generated by the large particles. Nevertheless, the data from video analysis is in general agreement with that obtained from the filtering method (Nicollier et al., 2021b, in review).

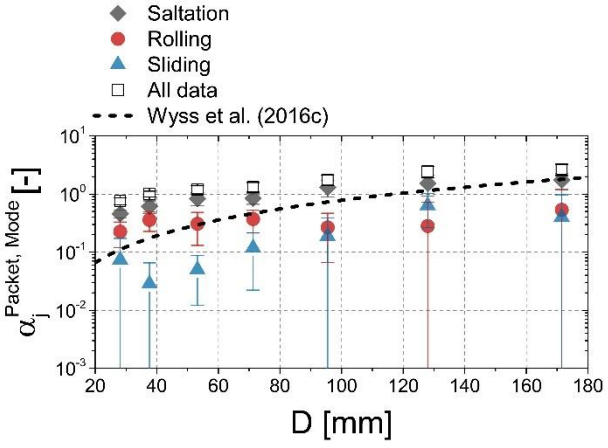

Figure 11: The number of packets divided by the number of transported particles for each transport mode ($\alpha_j^{Packet,Mode}$) as a function of bedload particle size *D* ranging from 28.1 mm to 171.5 mm. "All data" represents the sum of the packets generated by saltation, rolling and sliding particles. The results from the flume experiments are also compared to the data of the Erlenbach field measurements analyzed by Wyss et al. (2016a) for a mean flow velocity of 5 m/s.

The ratio $\alpha_j^{Packet,Mode}$ represents the number of packets (identified from the SPG signal) divided by the number of particles transported over the channel bed (Wyss et al., 2016c). This represents a detection probability and can be considered as a calibration curve of the SPG system, providing the values of $\alpha_j^{Packet,Mode}$ as a function of bedload particle size for each transport mode (**Fig. 11)**. For the transport mode of saltation, the larger particles generally generate more packets recorded by the SPG system due to the higher impact energy leading to the longer wave transport distance. The values of $\alpha_j^{Packet,Mode}$ of the rolling and sliding particles change less with increasing particle size (**Fig. 11**), and they are relatively smaller than the

https://doi.org/10.5194/esurf-2021-72
Preprint. Discussion started: 19 October 2021


Earth Surface Dynamics Discussions Open Access EGU

values for the saltation particles over all bedload particle size classes. This is likely due to the fact that, in this study, the bed shear stress is a constant during the flume experiments and is considerably larger than the critical bed shear stress, leading to a dominant transport mode of saltation.

The results obtained from the field measurements at the Erlenbach (Wyss et al., 2016) were compared with the results of our controlled flume experiments, showing relatively smaller values than the overall data and the saltation data based on the video analysis. However, the differences between the field measurements data and the overall packets data of the flume experiments decrease with increasing particle size. It indicates that for the transport conditions in the Erlenbach, saltation appears to the dominant mode for D > ca. 90 mm, while for D < ca. 90 mm, the larger flow velocity at the Erlenbach could be the reason for less signal response there as compared to the Obernach flume data. Note that the field measurements conducted by Wyss et al. (2016) were associated with a mean water flow velocity of 5 m/s which is higher than the 3.3 m/s in our flume experiments. As a consequence, the hop distance of a bedload particle in flow direction should be considerably larger for the field measurements than for the flume experiments, making it more likely for particles to fly over the plates, therefore, leading to the relatively smaller value of $\alpha_j^{Packet,Mode}$.

4.1.2 Impulses per particle mass

The impulse-mass coefficient k_{IPM} decreases differently with increasing particle size for the different transport modes of saltation, rolling and sliding. Generally, more impulses are triggered by the mode of saltation regardless of bedload particle size (**Fig. 8a**). This is possibly because the saltation particles have relatively higher hop heights and vertical impact velocities compared to the modes of rolling and sliding, under the same flow condition. The differences in k_{IPM} between the rolling and sliding become significant with larger bedload particle sizes. This could be due to the following reasons: (i) For the packets data that were used to calculate k_{IPM} it must be noted that the impact locations of bedload particles are variable, leading to the differences between the rolling and sliding particles. (ii) The shape of large sliding particles is flatter than of the rolling particles, which may also contribute differently to the signal impulses.

4.1.3 Maximum amplitude

The maximum amplitude of a packet $Amp_{Max,Pac}$ is growing in nearly a power law form with increasing particle size for all the transport modes, especially for the modes of saltation and rolling (**Fig. 9a**). However, the values of $Amp_{Max,Pac}$ increase less with changing bedload size for the largest particle sizes ranging from 127.9 mm to 171.5 mm, showing a qualitative agreement with the experiments at the Erlenbach (Wyss et al., 2016a) and with the FEM simulation data (Chen et al., 2021). The reason for this "saturation" limit in terms of maximum amplitude of a packet is likely due to a mechanical behavior of the SPG system. The variation of signal amplitude for each particle size class and each transport mode is mainly considered to be caused by particle impact location on the SPG plates because of flowing water. Experimental results determined from laboratory drop tests and numerical data obtained from FEM simulations showed that the maximum amplitude was reduced by more than 50% with changes from centric impacts to the eccentric impacts (Chen et al., 2021). Note that even within a

https://doi.org/10.5194/esurf-2021-72
Preprint. Discussion started: 19 October 2021

given particle size class in the flume experiments, the particles have a variable natural shape, which could also cause variable signal responses.

The median value of $Amp_{Max,Pac}$ for the mode of saltation is larger than that for the rolling and significantly larger than for the sliding particles (**Fig. 9**). This is because a particle in saltation generally has a higher impact velocity and can transfer more impact energy to the SPG plate. A considerable difference of $Amp_{Max,Pac}$ between the transport modes could potentially be helpful in identifying sliding particles and therefore may improve the signal conversion into fractional bedload transport rates.

4.1.4 Centroid frequency

The frequency $Freq_{Centroid}$ of a generated signal decreases with increasing bedload particle size (**Fig. 10a**), showing an agreement with previous investigations (Rickenmann, 2017; Wyss et al., 2016a). The median value of $Freq_{Centroid}$ for saltation particles is slightly larger than that for rolling and sliding particles. Assuming that the vertical impact velocity generally decreases from saltation to rolling to sliding particles, the observed change in $Freq_{Centroid}$ with changing transport mode is in general agreement with the Hertz theory (Thorne, 1985). However, for a given particle size class, the differences of $Freq_{Centroid}$ between all transported modes are not very significant. In any case, among all contributing factors, particle size dominates the centroid frequency according to the Hertz theory. Although all signal data were obtained under a constant flowing condition, the velocity of saltation particles is relatively larger but not considerably larger than that in rolling and sliding. The rolling and sliding bedload particles with approximately the same impact velocity move near the flume bed, resulting in little difference in frequency for the same size class.

4.2 Effect of particle impact angle on the SPG signal response

The impact angle θ between the directions of the water flow and the bedload particle motion might have an influence on the signal responses of the SPG system because of the changes of the vertical and horizontal components of impact velocity. The impulse-mass coefficient k_{IPM} changes only moderately with increasing impact angle ranging from around 5° to 90° as seen in numerical results (**Fig. 8b**), which were compared with the inclined chute experiments with both spherical and natural particles for the impact angles of 45° and 60°. However, a clear effect of bedload particle size on k_{IPM} can be observed in **Fig. 8b**, indicating that the value of k_{IPM} is reduced with increasing particle size, which shows a reasonable agreement with previous findings (Chen et al., 2021). This means that the SPG monitoring system is more sensitive to the bedload particle size than to the impact angle, in agreement with the Hertz theory as indicated above.

The maximum amplitude $Amp_{Max,Pac}$ increases with increasing impact angle for the numerical data up to an intermediate angle of about 45° (**Fig. 9b**). The values of $Amp_{Max,Pac}$ for the FEM simulations are considerably larger than those from the chute experiments for the impact angles of 45° and 60°. This may be partly because that the impact velocities in the inclined chute experiments were overestimated. Note that the impact velocities calculated from the experimental videos were variable even for a fixed release height and particle size, due to friction along the chute bed and drag forces of the water. The curves

https://doi.org/10.5194/esurf-2021-72
Preprint. Discussion started: 19 October 2021

of $Amp_{Max,Pac}$ to impact angle tend to become flatter with increasing impact angle. This is possibly due to a plastic behavior of the plate material, as the vertical velocity component becomes relatively large compared to typical natural flow conditions. For a given impacting sphere size, the centroid frequency $Freq_{Centroid}$ appears to be relatively insensitive to changing impact angle except for nearly horizontal impacts (**Fig. 10b)**. $Freq_{Centroid}$ is comparatively lower for impact angles ranging from 0° to 10° than for the rest of impact angles, which can be possibly explained as follows. We consider the fact that the horizontal impacts (sliding mode) in the FEM simulations are under a perfect condition with an impacting angle of 0°, indicating that a contact between the spherical particle and the SPG plate is dominated by friction. It's convenient to assume that as the impact angle approaches horizontal, the normal stress goes down while the shear stress increases. Furthermore, $Freq_{Centroid}$ can drop due to the extremely low vertical impact velocity (see **Tab. 3**) for the horizontal impact. As a consequence, the signal response and wave propagation could be fundamentally different with the circumstances of non-horizontal impacts, leading to a lower signal centroid frequency.

4.3 Comparison with other flume studies

4.3.1 Probability of transport mode

The probability of occurrence of each transport mode is related to the flow intensity or the transport stage (Auel et al., 2017; Hu and Hui, 1996a), indicating correlations with the bedload size as well. In the flume experiments conducted by Auel et al. (2017), sediment particles of three size categories, namely small, medium and large, ranging from about 5.3 mm to 17.5 mm were investigated in an artificial channel and recorded using the high-speed camera. Subsequently, the regression line that represents a shift from the saltation mode to the rolling mode was obtained, considering partial data from Hu and Hui (1996a), as seen in **Fig. 12a**. It is worth noting that the definition of the probability for the rolling mode is the ratio of the travelled distance by a rolling particle to the overall distance determined by the sum of saltation and rolling modes averaged over numbers of particles travels (Auel et al., 2017). Comparably, the data in our study is considered as the fraction calculated by the number of particles (or packets) represented by each transport mode, a similar definition as used by Hu and Hui (1996a).

The probability of rolling mode P_{Rol} decreases in a power law form with increasing excess transport stage T for the data compiled by Auel et al. (2017), as is also illustrated with their proposed power law model to distinguish between the rolling and saltation regions in **Fig. 12a.** In our study, the dominant transport mode is saltation, for P_{Sal} equals about 55% to 73% varying in T. In contrast, 12% to 37% of the particles are in rolling mode, followed by the sliding mode that shows about 6% to 23%. The changes in the probabilities of each transport mode are due to the effect of particle size D (or particle weight) ranging from 28.1 mm to 171.5 mm that leads to values of T changing from 6.42 to 0.22. With regard to P_{Rol}, the results of the flume experiments in Auel et al. (2017) indicated that large particles have a high probability P_{Rol}. This is likely because the percentage of energy consumption (induced by turbulence and friction) for the small particles is considerably larger than that for the large particles with high inertia. However, our experimental data show that P_{Rol} decreases as particle size

https://doi.org/10.5194/esurf-2021-72
Preprint. Discussion started: 19 October 2021


Earth Surface Dynamics Discussions
Open Access
EGU

increases, which may be related to the influence of gravity becoming important. Note that the particle size used in our experiments (**Tab. 1**) is approximately 5 to 10 times larger than the particles of Auel et al. (2017), resulting in a particle weight of about 125 to 1000 times larger in the former than in the latter. For the rolling particles and part of the saltation particles of our study, the experimental data are reasonably consistent with Auel et al. (2017). Interestingly, the probability of the sliding mode P_{Sli} displays an increase with increasing particle size, showing a different trend compared with the rolling mode. This is possibly due to the effect of particle shape: Flatter-shaped particles are more likely to move in the sliding mode, based on the video material. The shift from rolling to sliding could be estimated, as indicated by the regression line (blue dotted line) based on our flume observations in **Fig. 12a**. However, experiments considering more flow conditions are required to develop a more accurate model.

4.3.2 Particle velocity

Our experimental data for the dimensionless particle velocity V_P^* show a dependency on the transport stage T, indicating a power law (**Fig. 12b**). A similar trend was found by Auel et al. (2017), who compared their data with experimental data from other studies (Abbott and Francis, 1997; Ancey et al., 2008; Chatanantavet, 2007; Chatanantavet et al., 2013; Fernandez Luque and Van Beek, 1976; Hu and Hui, 1996; Ishibashi and Isobe, 1968; Lee and Hsu, 1994; Lajeunesse et al., 2010; Sekine and Kikkawa, 1992). V_P^* represents the particle velocity V_P ($V_P^{Cal,*}$ and $V_P^{Est,*}$) normalized by the term $\sqrt{(s-1)gD}$, where $V_P^{Cal,*}$ is the particle velocity calculated by particle travel distance and arrival time difference determined from the starting time of the packets of the SPG and MPA signals; $V_P^{Est,*}$ is the estimated particle velocity, assuming that the ratio (30% to 80%, the red shaded area in **Fig. 12b**) of particle velocity to the flow velocity is known.

Our results indicate that the estimated particle velocity is in the range of about 53% to 88% of the flow velocity, showing that it is slightly higher than but basically agrees with the range (the red shaded area in **Fig. 12b**) given in Julien and Bounvilay (2013). The data are also close to the empirical model presented by Auel et al. (2017), with the largest deviation for the lowest T. The general agreement of experimental data on particle velocities suggests that our observations on particle transport modes should also be comparable with other flume studies.

https://doi.org/10.5194/esurf-2021-72
Preprint. Discussion started: 19 October 2021

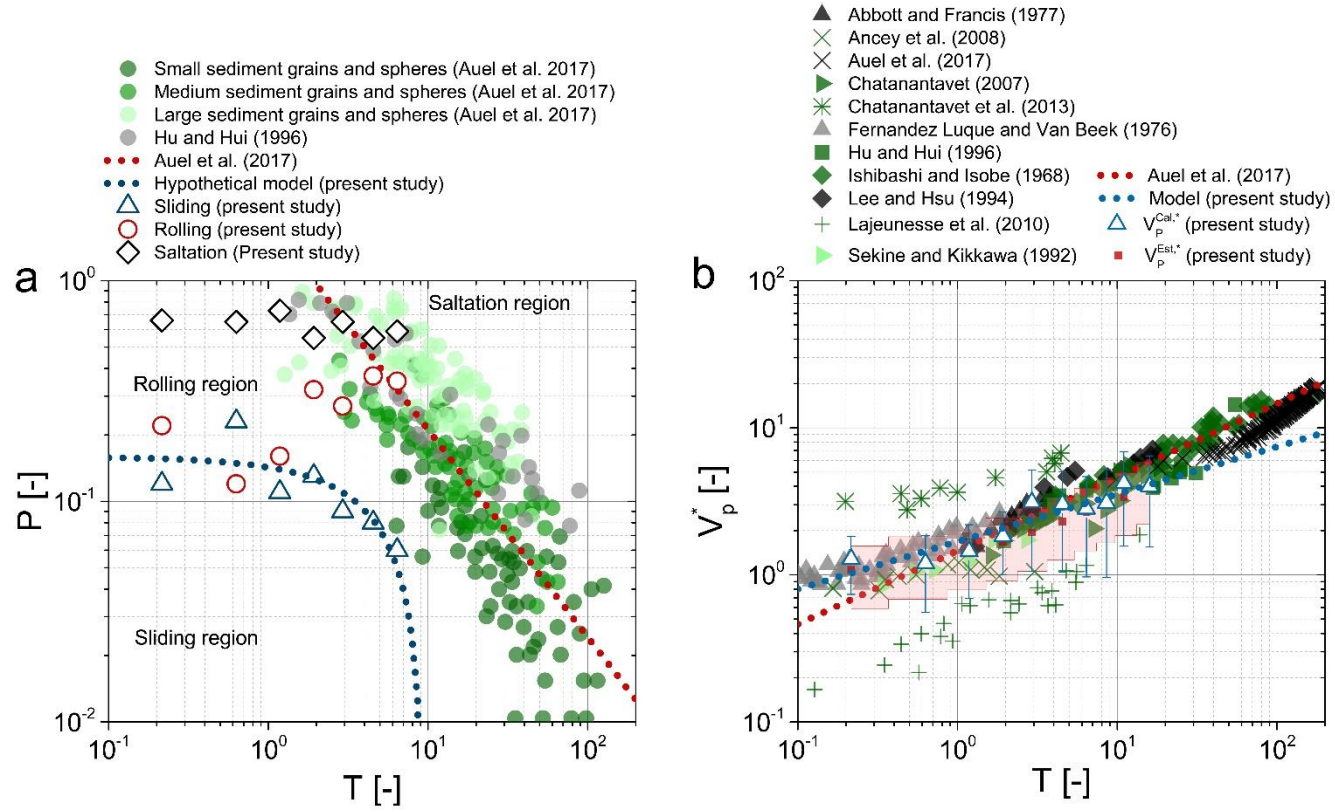

Figure 12: (a) Probability of transport mode P (P_{Sal} for saltation, P_{Rol} for rolling, and P_{Sli} for sliding) as functions of the excess transport stage T. The data from Auel et al. (2017), associated with natural grains and spheres with variable sizes ranging from about 5.3 mm to 17.5 mm, are shown in green. The data from Hu and Hui (1996a) are presented in gray. The present results from our flume experiments in terms of T ranging from 0.22 to 6.42 are compared to the power law model $\boldsymbol{P = 1.84T^{-0.94}}$ applied by Auel et al. (2017) (red dotted line), with R^2 = 0.64, and their compiled data. The (hypothetical) model $\boldsymbol{P = -0.017T + 0.16}$, given by the blue dotted line, represents a suggested boundary between the sliding and rolling regions based on our flume observations. (b) The non-dimensional particle velocity $\boldsymbol{V_P^* = V_P/\sqrt{(s-1)gD}}$ versus T. The power law model $\boldsymbol{V_P^* = 1.46T^{0.5}}$ applied by Auel et al. (2017) is shown in red dotted line, with R^2 = 0.95. The blue dotted line, $\boldsymbol{V_P^* = 1.68T^{0.32}}$, R^2 = 0.87, is based on our experimental data.

5 Conclusions

In this research, systematic flume experiments and FEM simulations were conducted to study the signal response of the Swiss plate geophone bedload monitoring system when impacted by natural bedload particles varying in size, and showing different angles of impact and transport modes. Some key parameters of the acoustic signal have been analyzed, including the ratio of the number of packets to the number of transported particles $\alpha_j^{Packet,Mode}$, the maximum amplitude of a packet $Amp_{Max,Pac}$, the impulse-mass coefficient k_{IPM}, and the centroid frequency $Freq_{Centroid}$. The major conclusions of this study are summarized as follows:

[1] The number of impacts counted from the experimental video is in general agreement with the data obtained from the

https://doi.org/10.5194/esurf-2021-72
Preprint. Discussion started: 19 October 2021

filtering method. The number of packets for the rolling and sliding particles changes less with increasing particle size. Also, for all bedload particle size classes, sliding and rolling generate less packets than saltation.

[2] The number of signal impulses per unit particle mass decreases nonlinearly with increasing bedload particle size, and displays a dependency on particle transport mode. It only weakly depends on particle impact angle. In general, saltating particles trigger a larger number of signal impulses than rolling and sliding particles.

[3] The maximum amplitude of a signal packet increases with increasing particle size for the saltating and rolling particles, showing a dependency on particle impact angle. The strongest signal response of the SPG system is excited by the saltation particles, followed by the rolling particles, and the weakest signal is triggered by the sliding particles.

[4] The centroid frequencies of the acoustic signal generally decrease with increasing particle size across all transport modes. For the FEM simulations, the centroid frequency values are considerably lower for the horizontal impact than for the rest of impact angles for a given particle size, indicating differences between the sliding and the saltation particles.

[5] The probability of each transport mode correlates with the transport stage and particle size of the bedload. The dominant transport mode in this study is saltation, and the data indicate a possible threshold between the modes of rolling and sliding. The non-dimensional velocity of bedload particle increases in a power law form with increasing transport stage, and is in general agreement with other flume studies.

Appendix A

The analysis of the experimental videos included the following five steps: (1) tracking a saltating bedload particle from frame to frame during a certain time duration, especially when the particle contacts with the SPG plate or a nearby location, because saltation generally triggers a higher signal amplitude than the other two transport modes; (2) determining the time instants (time series T_m^V) of each impact caused by this particle from the video frames, including the observation of a slight rotation (at time $T_{m_0}^V = T_2$) of the particle at the contact point, as described above; (3) isolating the signal packet (at time $T_{i_0}^S$) from the SPG output signals, as this packet is indicative of the particle impact on the SPG plates; (4) matching the analyzed particle impacts with the SPG signals, using the formula **Eq. A1** and satisfying the condition of **Eq. A2**; (5) checking the impact instants generated by the rolling and sliding particles.

$$T_i^{S,Cal} = \lambda\left(T_m^V - T_{m_0}^V\right) + T_{i_0}^S \,, \tag{A1}$$

$$\left|T_i^S - T_i^{S,Cal}\right| < 3 \times 10^{-3} \text{ sec} \,, \tag{A2}$$

where λ = 1/3 is a coefficient for correcting the video time, $T_i^{S,Cal}$ is the calculated time instant for each signal packet, T_m^V is the time instant of each bedload impact based on video observation, $T_{m_0}^V$ is the representative impact instant based on video observation, $T_{i_0}^S$ is the time instant for the isolated signal packet matched with $T_{m_0}^V$, and T_i^S is the packets' time series

https://doi.org/10.5194/esurf-2021-72
Preprint. Discussion started: 19 October 2021


Earth Surface Dynamics Discussions
Open Access
EGU

recorded by geophones. The upper limit is considered in **Eq. A2** because, in general, the contact time between the particle and the plate ranges from one to three milliseconds, which is less than the packet duration that typically lasts five to ten milliseconds.

Appendix B

Figs. B1a and **B1b** show representative signals of the SPG and MPA systems. The arrival time difference $\Delta T_P^{SPG,MPA}$ between the systems can be calculated from the starting time of the packets T_P^{SPG} and T_P^{MPA} for the SPG and MPA as $\Delta T_P^{SPG,MPA} = T_P^{MPA} - T_P^{SPG}$, noting that the MPA system is located at the downstream position of the SPG system Thus, the question now is to determine T_P^{SPG} and T_P^{MPA}.

Given a time window T^W and time step Δt_P (as seen in **Figs. B1a** and **B1b**), the number of packets P^{W_k} within the k^{th} time window T_k^W can be counted as:

$$P^{W_k} = \sum_1^n m^{W_k}, \tag{B1}$$

where k = 1, 2, …, $\left\lfloor \frac{T^E - T^W}{\Delta t_P} \right\rfloor$; T^E is time duration of an experiment; "⌊ ⌋" is the ceiling operator; n is the value of number of packets P^{W_k}, varying with the moving time window; m = 1.

In our study, the time window and time step are given as 1.0 s and 0.05 s, respectively. Consequently, the number of packets for the SPG and MPA system over the experimental duration T^E can be expressed as functions of time, corresponding to the blue and red lines in **Figs. B1c** and **B1d**, respectively. As the final number, we utilize the time difference that accounts for 5% of the maximum value, as seen below:

$$\Delta T_P^{SPG,MPA} = T_P^{MPA,5th} - T_P^{SPG,5th}, \tag{B2}$$

where $T_P^{MPA,5th}$ and $T_P^{SPG,5th}$ correspond to 5% of the maximum value in **Fig. B1c**.

https://doi.org/10.5194/esurf-2021-72
Preprint. Discussion started: 19 October 2021

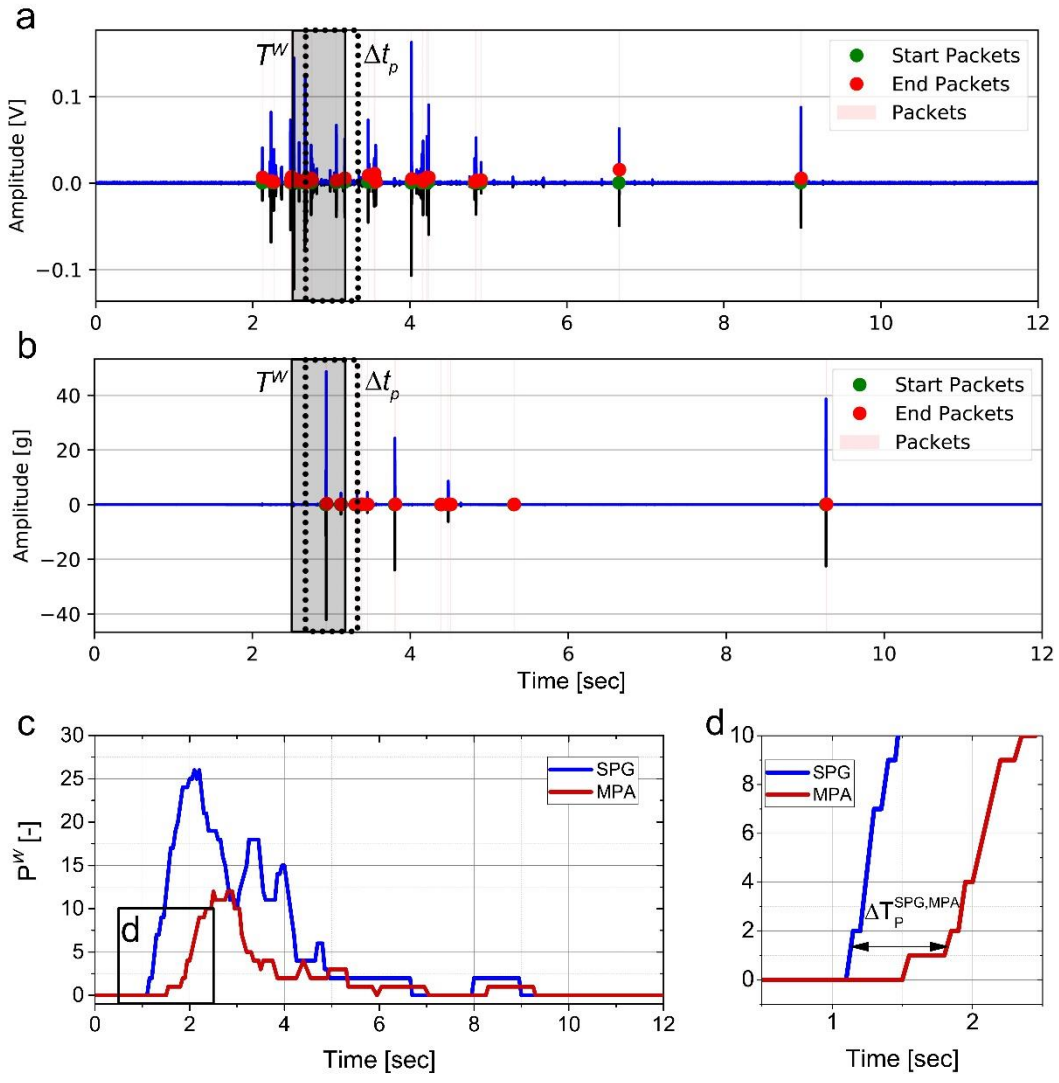

Figure B1: Illustration of the vibrations, signal packets and counts of packet number, following a flume experiment with bedload particles of grain-size class C4 and with a flow velocity of 3.3 m/s. (a) and (b) are representative signals that were recorded by the SPG and MPA systems, respectively. (c) and (d) Counting the number of packets, summing up the numbers within the given time window (grey shaded area in (a) and (b)). The blue and red lines are the summed number of packets of each time window for the SPG and MPA systems, respectively.

Code availability statement

Please contact Dieter Rickenmann (dieter.rickenmann@wsl.ch) and Tobias Nicollier (tobias.nicollier@wsl.ch) if readers are interested in the code used in this paper.

https://doi.org/10.5194/esurf-2021-72
Preprint. Discussion started: 19 October 2021

Data availability statement

Datasets for this research are available upon request to the readers.

Author contribution

Zheng Chen: Formal analysis, Investigation, Methodology, Software, Visualization, Writing – original draft preparation, Writing – review & editing; **Siming He:** Software, Writing – review & editing; **Tobias Nicollier:** Data curation, Investigation, Methodology, Software, Writing – review & editing; **Lorenz Ammann:** Investigation, Writing – review & editing; **Alexandre Badoux:** Supervision, Writing – review & editing; **Dieter Rickenmann:** Conceptualization, Funding acquisition, Resources, Supervision, Validation, Writing – review & editing.

Competing interest

The authors declare that they have no conflict of interest.

Funding information

This study was supported by the National Natural Science Foundation of China (grants 41772312 and 41790433 awarded to SH), the Key Deployment Project of CAS (grant KFZD-SW-424 awarded to SH), the China Scholarship Council CSC (file no. 201904910867 awarded to ZC), and the Swiss National Science Foundation SNSF (grant 200021L_172606 awarded to DR).

Acknowledgement

We thank Arnd Hartlieb and his colleagues of TU Munich for their support with the experiments in the Obernach outdoor flume facility.

Notations

Symbols	Descriptions
$T_{i_0}^S$	time instant for an isolated signal packet [s]
$T_{m_0}^V$	representative impact instant based on video observation [s]
$A_{FFT,\,m}$	amplitude that is obtained by performing fast Fourier transform FFT on the signals [V·s]
$Amp_{Max,Pac}$	maximum positive amplitude of the packet [V]

https://doi.org/10.5194/esurf-2021-72
Preprint. Discussion started: 19 October 2021

b	channel width [m]
D_i	mean value of bedload particle diameter for each size class i [mm]
$\boldsymbol{F_c}$	friction force exerted by the SPG plate on the bedload particle [N]
$F_{Contact}$	contact force between the sphere and the plate [N]
FEM	finite element method [-]
FFT	fast Fourier transform [-]
f_m	spectrum frequency [Hz]
$\boldsymbol{F_n}$	vertical support force exerted by the SPG plate on the bedload particle [N]
FPS	frames per second [s^{-1}]
$Freq_{centroid}$	centroid frequency of acoustic signals [Hz]
$\boldsymbol{F_w}$	force of water acting on the bedload particle [N]
$\boldsymbol{G}$	particle weight force [N]
g	gravity acceleration [m s^{-2}]
h	flow depth [m]
I	number of impulses recorded by the SPG system for each impact event [-]
I_j	impulses recorded by the SPG system for bedload particle-size class j [-]
JPM	the Japanese pipe microphone [-]
k_{IPM}	number of impulses per particle mass that is transported [kg^{-1}]
L_P	particle travel distance [m]
$L_P^{SPG,MPA}$	centre-to-centre distance between the SPG and MPA systems [m]
m	Number of tests [-]
M	transported bedload mass [kg]
M_j	mean value of bedload particle mass for each size class j [kg]
MPA	the miniplates accelerometer [-]
n	number of particles for each experimental run [-]
$N_{i,j}$	number of particles for each experimental run i and grain-size class j [-]
$N_{i,j}^{Mode}$	number of particles for experimental run i and particle-size class j for the transport mode of saltation, rolling and sliding [-]
$N_{i,j}^{Packet,F}$	number of real packets for experimental run i and particle-size class j determined by the filtering method [-]
$N_{i,j}^{Packet,V}$	total number of real packets for experimental run i and particle-size class j for all transport modes based on the video analysis [-]
P^{W_k}	number of packets within the k^{th} time window [-]
$P_{i,j}$	number of packets for each experimental run i and grain-size class j [-]
$P_{i,j}^{Mode}$	number of packets for experimental run i and particle-size class j for the motion mode of saltation, rolling and sliding [-]
P_M	probability of transport mode (P_{Sal}, P_{Rol}, and P_{Sli} for saltation, rolling, and sliding, respectively) [-]
R_h	hydraulic radius [m]
$r_{i,j}^{Packet,V\_F}$	ratio of the total number of real packets for all transport modes based on the video observations to the number of real packets for experimental run i and particle-size class j determined by numerical filtering method [-]

https://doi.org/10.5194/esurf-2021-72
Preprint. Discussion started: 19 October 2021

r_{PW}	ratio of particle velocity to water flow velocity [-]
S	bed slope [-]
s	ratio of particle density to water density
SPG	the Swiss plate geophone [-]
T	excess transport stage [-]
T^E	time duration of an experiment [-]
T_i^S	packets' time series recorded by geophones [s]
$T_i^{S,Cal}$	calculated time instant for each signal packet [s]
T_k^W	The k^{th} time window [s]
T_m^V	time instant of each bedload impact based on video observation [s]
T_P^{MPA}	starting time of the packets for the MPA system [s]
$T_P^{MPA,5th}$	starting time of the packets for the SPG system, corresponding to 5% of the maximum value [s]
$T_P^{MPA,5th}$	starting time of the packets for the MPA system corresponding to 5% of the maximum value [s]
T_P^{SPG}	starting time of the packets for the SPG system [s]
T^W	time window [s]
V	impact velocity of the sphere onto the plate [m s^{-1}]
V_P	particle velocity [m s^{-1}]
V_P^*	dimensionless particle velocity [-]
V_P^{Cal}	calculated particle velocity [m s^{-1}]
$V_P^{Cal,*}$	particle velocity calculated by particle travel distance and time lag determined from the SPG and MPA signals [-]
V_P^{Est}	estimated particle velocity [m s^{-1}]
$V_P^{Est,*}$	particle velocity estimated from the ratio of the averaged particle velocity to water flow velocity [-]
$V_P^{M,*}$	nondimensional particle velocity $V_P^{Est,*}$ or $V_P^{Cal,*}$ [-]
V_W	water flow velocity [m s^{-1}]
V_Y	Y-component of the impact velocity [m s^{-1}]
V_Z	Z-component of the impact velocity [m s^{-1}]
$\alpha_{i,j}^{Packet}$	ratio of the number of packets to the number of particles for each experimental run i and grain-size class j [-]
$\alpha_{i,j}^{Packet,Mode}$	ratios of the number of packets to the number of particles for experimental run i and particle-size class j for the motion mode of saltation, rolling and sliding [-]
ΔT_P	particle travel time [s]
Δt_P	time step [s]
$\Delta T_P^{SPG,MPA}$	arrival time difference determined from the starting time of the packets and for the SPG and MPA systems [s]
θ	impact angle [°]
$\Theta_{Critical}$	critical Shields parameter [-]
λ	coefficient for correcting the video time [-]
ρ	water density [kg m^{-3}]

https://doi.org/10.5194/esurf-2021-72
Preprint. Discussion started: 19 October 2021

ρ_s	particle density [kg m^{-3}]
$\overline{\tau_b}$	time-averaged bed shear stress [N m^{-2}]
$\tau_{critical}$	critical bed shear stress [N m^{-2}]

References

Abbott, J. E., and Francis, J. R. D.: Saltation and suspension trajectories of solid grains in a water stream, Philos. Trans. A. Math. Phys. Sci., 284.1321, 225-254, https://doi.org/10.1098/rsta.1977.0009, 1977.

Ancey, C., Davison, A. C., Böhm, T., Jodeau, M., and Frey, P.: Entrainment and motion of coarse particles in a shallow water stream down a steep slope, J. Fluid Mech., 595, 83-114, https://doi.org/10.1017/S0022112007008774, 2008.

Antoniazza, G., Nicollier, T., Wyss, C. R., Boss, S., and Rickenmann, D.: Bedload transport monitoring in Alpine rivers: variability in Swiss plate geophone response, Sensors, 20, 4089, https://doi.org/10.3390/s20154089, 2020.

Auel, C., Albayrak, I., Sumi, T., and Boes, R. M.: Sediment transport in high-speed flows over a fixed bed: 1. Particle dynamics, Earth. Surf. Process. Landf., 42, 1365-1383, https://doi.org/10.1002/esp.4128, 2017.

Barton, J. S., Slingerland, R. L., Pittman, S., and Gabrielson, T. B.: Monitoring coarse bedload transport with passive acoustic instrumentation: A field study, US Geol. Surv. Sci. Investig., Rep, 5091, 14 pp., 2010.

Barton, J. S., Slingerland, R. L., Pittman, S., and Gabrielson, T. B.: Passive acoustic monitoring of coarse bedload transport on the Trinity River, Eighth Federal Interagency Sedimentation Conference, 2-6 April 2006, 627-634, https://pubs.usgs.gov/misc/FISC_1947-2006/pdf/1st-7thFISCs-CD/8thFISC/Session%209C-3_BartonEtAl.pdf, 2006.

Beylich, A. A., and Laute, K.: Combining impact sensor field and laboratory flume measurements with other techniques for studying fluvial bedload transport in steep mountain streams, Geomorphology, 218, 72–87, https://doi.org/10.1016/j.geomorph.2013.09.004, 2014.

Bunte, K., Abt, S. R., Potyondy, J. P., and Ryan, S. E.: Measurement of coarse gravel and cobble transport using portable bedload traps, J. Hydraul. Eng., 130, 879–893, https://doi.org/10.1061/(ASCE)0733–9429(2004)130:9(879), 2004.

Burtin, A., Bollinger, L., Vergne, J., Cattin, R., and Nábělek, J. L.: Spectral analysis of seismic noise induced by rivers: A new tool to monitor spatiotemporal changes in stream hydrodynamics, J. Geophys. Res. Solid Earth, 113, https://doi.org/10.1029/2007JB005034, 2008.

Burtin, A., Cattin, R., Bollinger, L., Vergne, J., Steer, P., Robert, A., Findling, N., and Tiberi, C.: Towards the hydrologic and bed load monitoring from high–frequency seismic noise in a braided river: The “torrent de St Pierre”, French Alps, J. Hydrol., 408, 43–53, https://doi.org/10.1016/j.jhydrol.2011.07.014, 2011.

https://doi.org/10.5194/esurf-2021-72
Preprint. Discussion started: 19 October 2021

Burtin, A., Vergne, J., Rivera, L., and Dubernet, P.: Location of river–induced seismic signal from noise correlation functions, Geophys. J. Int., 182, 1161–1173, https://doi.org/10.1111/j.1365–246X.2010.04701.x, 2010.

Camenen, B., Jaballah, M., Geay, T., Belleudy, P., Laronne, J. B., and Laskowski, J. P.: Tentative measurements of bedload transport in an energetic alpine gravel bed river, In River flow, September 2012, 379–386, https://hal.inrae.fr/hal–02597879, 2012

Cassel, M., Lavé, J., Recking, A., Malavoi, J. R., and Piégay, H.: Bedload transport in rivers, size matters but so does shape. Sci. Rep., 11, 1-11, https://doi.org/10.1038/s41598-020-79930-7, 2021.

Chatanantavet, P., Whipple, K. X., Adams, M. A., and Lamb, M. P.: Experimental study on coarse grain saltation dynamics in bedrock channels, J. Geophys. Res. Earth Surface, 118, 1161-1176, https://doi.org/10.1002/jgrf.20053, 2013.

Chatanantavet, P.: Physically-based models of bedrock incision processes in mountain streams, Ph.D. thesis, University of Minnesota, Minneapolis, USA, 210 pp., 2007.

Chen, Z., He, S., Nicollier, T., Ammann, L., Badoux, A., and Rickenmann, D.: Controlled experiments and finite element simulations with the Swiss plate geophone bedload monitoring system: particle size identification and transport mode, EGU General Assembly 2021, online, 19–30 Apr 2021, EGU21-2078, https://doi.org/10.5194/egusphere-egu21-2078, 2021.

Childers, D.: Field comparisons of six pressure–difference bedload samplers in high–energy flow, US Department of the Interior, US Geological Survey, URL, 71 pp., 1999.

Emmett, W. W.: A field calibration of the sediment–trapping characteristics of the Helley–Smith bedload sampler, US Government Printing Office, 54 pp., 1980.

Farin, M., Tsai, V. C., Lamb, M. P., and Allstadt, K. E.: A physical model of the high-frequency seismic signal generated by debris flows, Earth. Surf. Process. Landf., 44, 2529–2543, https://doi.org/10.1002/esp.4677, 2019.

Fernandez Luque, R., and Van Beek, R.: Erosion and transport of bed-load sediment, J. Hydraul. Res., 14, 127-144, https://doi.org/10.1080/00221687609499677, 1976.

Geay, T., Belleudy, P., Gervaise, C., Habersack, H., Aigner, J., Kreisler, A., Seiz, H., and Laronne, J. B.: Passive acoustic monitoring of bed load discharge in a large gravel bed river, J. Geophys. Res. Solid Earth, 122, 528–545, https://doi.org/10.1002/2016JF004112, 2017.

Gimbert, F., Fuller, B. M., Lamb, M. P., Tsai, V. C., and Johnson, J. P.: Particle transport mechanics and induced seismic noise in steep flume experiments with accelerometer-embedded tracers, Earth. Surf. Process. Landf., 44, 219–241, https://doi.org/10.1002/esp.4495, 2019.

Govi, M., Maraga, F., and Moia, F.: Seismic detectors for continuous bed load monitoring in a gravel stream, Hydrol. Sci. J., 38, 123–132, https://doi.org/10.1080/02626669309492650, 1993.

Gray, J. R., Laronne, J. B., and Marr, J. D.: Bedload–surrogate monitoring technologies, US Department of the Interior, US Geological Survey, 37 pp., 2010.

Habersack, H. M., and Laronne, J. B.: Evaluation and improvement of bed load discharge formulas based on Helley–Smith sampling in an alpine gravel bed river, J. Hydraul. Eng., 128, 484-499, https://doi.org/10.1061/(ASCE)0733-9429(2002)128:5(484), 2002.

Hayward, J. A.: Hydrology and stream sediments in a mountain catchment, Lincoln College, Tussock Grasslands and Mountain Lands Institute, http://researcharchive.lincoln.ac.nz/handle/10182/5664, 1980.

Helley, E. J., and Smith, W.: Development and calibration of a pressure–difference bedload sampler, US Department of the Interior, Geological Survey, Water Resources Division, 38 pp., 1971.

Hsu, L., Finnegan, N. J., and Brodsky, E. E.: A seismic signature of river bedload transport during storm events, Geophys. Res. Lett., 38, https://doi.org/10.1029/2011GL047759, 2011.

Hu, C., and Hui, Y.: Bed-load transport. I: Mechanical characteristics, J. Hydraul. Eng., 122, 245-254, https://doi.org/10.1061/(ASCE)0733-9429(1996)122:5(245), 1996.

Ishibashi, T., Isobe, A.: Hydraulic study on the protection of erosion of sand flush channel (in Japanese), Central Research Institute of Electric Power Industry (CRIEPI), Rep. 67104, 1968.

Julien, P. Y., and Bounvilay, B.: Velocity of rolling bed load particles, J. Hydraul. Eng., 139, 177-186, https://doi.org/10.1061/(ASCE)HY.1943-7900.0000657, 2013.

Krein, A., Klinck, H., Eiden, M., Symader, W., Bierl, R., Hoffmann, L., and Pfister, L.: Investigating the transport dynamics and the properties of bedload material with a hydro-acoustic measuring system, Earth. Surf. Process. Landf., 33, 152-163, https://doi.org/10.1002/esp.1576, 2008.

Lajeunesse E, Malverti L, Charru F.: Bed load transport in turbulent flow at the grain scale: experiments and modelling, J. Geophys. Res. Earth Surface, 115, https://doi.org/10.1061/(ASCE)HY.1943-7900.0000657, 2010.

Lee, H. Y., and Hsu, I. S.: Investigation of saltating particle motions, J. Hydraul. Eng., 120, 831-845, https://doi.org/10.1061/(ASCE)0733-9429(1994)120:7(831), 1994.

LSTC.: LS–DYNA keyword user's manual, Livermore Software Technology Corporation, Livermore, California, http://www.lstc.com/, 2014.

https://doi.org/10.5194/esurf-2021-72
Preprint. Discussion started: 19 October 2021

Mizuyama, T., Oda, A., Laronne, J. B., Nonaka, M., and Matsuoka, M.: Laboratory tests of a Japanese pipe geophone for continuous acoustic monitoring of coarse bedload, US Geological Survey Scientific Investigations Report, 5091, 17 pp., 2010.

Møen, K. M., Bogen, J., Zuta, J. F., Ade, P. K., and Esbensen, K.: Bedload measurement in rivers using passive acoustic sensors, US Geological Survey Scientific Investigations Report, 5091, 17 pp., 2010.

Nicollier, T., Antoniazza, G., Rickenmann, D., and Hartlieb, A., Kirchner, J.W.: Improving the calibration of impact plate bedload monitoring systems by filtering out acoustic signals from extraneous particle impacts, ESSOAr [preprint], https://doi.org/10.1002/essoar.10507726.2, 13 August 2021b.

Nicollier, T., Rickenmann, D., and Hartlieb, A.: Calibration of the Swiss plate geophone system at the Albula field site with direct bedload samples and comparison with controlled flume experiments, SEDHYD 2019 Conference, Federal Interagency Sedimentation and Hydrologic, Modeling Conference. Reno, USA, 24-28 June 2019, 345, 2019.

Nicollier, T., Rickenmann, D., and Hartlieb, A.: Field and flume measurements with the impact plate: Effect of bedload grain-size distribution on signal response, Earth. Surf. Process. Landf., 46: 1504–1520, https://doi.org/10.1002/esp.5117, 2021a.

Nicollier, T., Rickenmann, D., Boss, S., Travaglini, E., and Hartlieb, A.: Calibration of the Swiss plate geophone system at the Zinal field site with direct bedload samples and results from controlled flume experiments, River Flow 2020, Proceedings of the 10th Conference on Fluvial Hydraulics, Delft, Netherlands, 7-10 July, 2020, 1-8, 2020.

Rickenmann, D., and Fritschi, B.: Bedload transport measurements with impact plate geophones in two Austrian mountain streams (Fischbach and Ruetz): system calibration, grain size estimation, and environmental signal pick–up, Earth Surf. Dyn., 5, 669–687, https://doi.org/10.5194/esurf–5–669–2017, 2017.

Rickenmann, D., and McArdell, B. W.: Continuous measurement of sediment transport in the Erlenbach stream using piezoelectric bedload impact sensors, Earth. Surf. Process. Landf., 32, 1362–1378, https://doi.org/10.1002/esp.1478, 2007.

Rickenmann, D., Turowski, J. M., Fritschi, B., Klaiber, A., and Ludwig, A.: Bedload transport measurements at the Erlenbach stream with geophones and automated basket samplers, Earth. Surf. Process. Landf., 37, 1000–1011. https://doi.org/10.1002/esp.3225, 2012.

Rickenmann, D., Turowski, J. M., Fritschi, B., Wyss, C., Laronne, J., Barzilai, R., Reid, I., Kreisler, A., Aigner, J., Seitz, H., and Habersack, H.: Bedload transport measurements with impact plate geophones: comparison of sensor calibration in different gravel-bed streams, Earth. Surf. Process. Landf., 39, 928–942, https://doi.org/10.1002/esp.3499, 2014.

https://doi.org/10.5194/esurf-2021-72
Preprint. Discussion started: 19 October 2021

Rickenmann, D.: Bed–load transport measurements with geophones and other passive acoustic methods, J. Hydraul. Eng., 143, 03117004, https://doi.org/10.1061/(ASCE)HY.1943–7900.0001300, 2017.

Rickenmann, D.: Effect of sediment supply on cyclic fluctuations of the disequilibrium ratio and threshold transport discharge, inferred from bedload transport measurements over 27 years at the Swiss Erlenbach stream, Water Resour. Res., 56, e2020WR027741, https://doi.org/10.1029/2020WR027741, 2020.

Rickenmann, D.: Methods for the quantitative assessment of channel processes in torrents (steep streams), CRC Press, 2016.

Rigby, J. R., Kuhnle, R. A., Goodwiller, B. T., Nichols, M. H., Carpenter, W. O., Wren, D. G., and Chambers, J. P.: Sediment–generated noise (SGN): Comparison with physical bed load measurements in a small semi–arid watershed, In SEDHYD Conference, April 2015, 19–23, 2015.

Rigby, J. R., Wren, D. G., and Kuhnle, R. A.: Passive acoustic monitoring of bed load for fluvial applications, J. Hydraul. Eng., 142, 02516003, https://doi.org/10.1061/(ASCE)HY.1943–7900.0001122, 2016.

Roth, D. L., Finnegan, N. J., Brodsky, E. E., Rickenmann, D., Turowski, J. M., Badoux, A., and Gimbert, F.: Bed load transport and boundary roughness changes as competing causes of hysteresis in the relationship between river discharge and seismic amplitude recorded near a steep mountain stream, J. Geophys. Res. Earth Surface, 122, 1182–1200, https://doi.org/10.1002/2016JF004062, 2017.

Ryan, S. E., Porth, L. S., and Troendle, C. A.: Coarse sediment transport in mountain streams in Colorado and Wyoming, USA, Earth. Surf. Process. Landf., 30, 269–288, https://doi.org/10.1002/esp.1128, 2005.

Schneider, J. M., Rickenmann, D., Turowski, J. M., Bunte, K., and Kirchner, J. W.: Applicability of bed load transport models for mixed-size sediments in steep streams considering macro-roughness, Water Resour. Res., 51, 5260-5283, https://doi.org/10.1002/2014WR016417, 2015.

Sekine M, Kikkawa H.: Mechanics of saltating grains II, J. Hydraul. Eng., 118, 536–558, https://doi.org/10.1061/(ASCE)0733-9429(1992)118:4(536), 1992.

Shahmohammadi, R., Afzalimehr, H., and Sui, J.: Assessment of Critical Shear Stress and Threshold Velocity in Shallow Flow with Sand Particles, Water, 13, 994. https://doi.org/10.3390/w13070994, 2021.

Thorne, P. D.: The measurement of acoustic noise generated by moving artificial sediments. J. Acoust. Soc. Am., 78, 1013-1023, https://doi.org/10.1121/1.393018, 1985.

Tsai, V. C., Minchew, B., Lamb, M. P., and Ampuero, J. P.: A physical model for seismic noise generation from sediment transport in rivers, Geophys. Res. Lett., 39, 1-6, https://doi.org/10.1029/2011GL050255, 2012.

Tsakiris, A. G., Papanicolaou, A. T. N., and Lauth, T. J.: Signature of bedload particle transport mode in the acoustic signal of a geophone, J. Hydraul. Res., 52, 185–204, https://doi.org/10.1080/00221686.2013.876454, 2014.

https://doi.org/10.5194/esurf-2021-72
Preprint. Discussion started: 19 October 2021

Turowski, J. M., and Rickenmann, D.: Tools and cover effects in bedload transport observations in the Pitzbach, Austria, Earth. Surf. Process. Landf., 34, 26–37. https://doi.org/10.1002/esp.1686, 2009.

Turowski, J. M., Böckli, M., Rickenmann, D., and Beer, A. R.: Field measurements of the energy delivered to the channel bed by moving bed load and links to bedrock erosion, J. Geophys. Res. Earth Surface, 118, 2438–2450, https://doi.org/10.1002/2013JF002765, 2013.

Turowski, J. M., Wyss, C. R., and Beer, A. R.: Grain size effects on energy delivery to the streambed and links to bedrock erosion, Geophys. Res. Lett., 42, 1775–1780, https://doi.org/10.1002/2015GL063159, 2015.

Vasile, G.: Vibration data processing for bedload monitoring in underwater environments, Remote Sens., 12, 2797, https://doi.org/10.3390/rs12172797, 2020.

Wyss, C. R., Rickenmann, D., Fritschi, B., Turowski, J. M., Weitbrecht, V., and Boes, R. M.: Laboratory flume experiments with the Swiss plate geophone bed load monitoring system: 1. Impulse counts and particle size identification, Water Resour. Res., 52, 7744–7759, https://doi.org/10.1002/2015WR018555, 2016a.

Wyss, C. R., Rickenmann, D., Fritschi, B., Turowski, J. M., Weitbrecht, V., Travaglini, E., Bardou, E., and Boes, R. M.: Laboratory flume experiments with the Swiss plate geophone bed load monitoring system: 2. Application to field sites with direct bed load samples, Water Resour. Res., 52, 7760–7778, https://doi.org/10.1002/2016WR019283, 2016b.

Wyss, C. R., Rickenmann, D., Fritschi, B., Turowski, J. M., Weitbrecht, V., and Boes, R. M.: Measuring bed load transport rates by grain–size fraction using the Swiss plate geophone signal at the Erlenbach, J. Hydraul. Eng., 142, 04016003, https://doi.org/10.1061/(ASCE)HY.1943–7900.0001090, 2016c.

Wyss, C. R., Rickenmann, D., Fritschi, B., Turowski, J. M., Weitbrecht, V., and Boes, R. M.: Bedload grain size estimation from the indirect monitoring of bedload transport with Swiss plate geophones at the Erlenbach stream, River Flow 2014, 1907-1912, 6 pp., 2014.